Future Design Flood Values in the Fraser and Peace River Basins Using the CanESM2-LE

Final Report to "Revision and Expansion of Extreme Streamflow Design Value Projection Online Tool"

Agreement Number # 820LA0008

March 30, 2023

Markus A. Schnorbus

Mohamed Ali Ben Alaya

Pacific Climate Impacts Consortium

Prepared for: Engineering Services Branch of the Engineering Systems Department of the Highway Services Department, Ministry of Transportation and Infrastructure, Government of British Columbia.

University of Victoria

Table of Contents

1 Introduction

Based on the BC Ministry of Transportation and Infrastructure (MoTI) led synthesis of Vulnerability Assessments, completed using the Public Infrastructure Engineering Vulnerability Committee (PIEVC) Protocol, climate change has increased risk to transportation infrastructure in BC (BCMoTI et al., 2014). To address this increased risk, the BCMoTI released directives and guidance for incorporating climate adaptation into engineering designs in its T-04/19 Technical Circular (BCMoTI, 2019). This guidance document stipulates transportation engineering design projects should "incorporate information, analyses and projections of the impact of future climate change and weather extremes". It also lists a few sources of climate change information such as the Pacific Climate Impacts Consortium's (PCIC's) analysis tools, including the Climate Explorer and Plan2Adapt.

To support the requirement for guidance on climate change impacts related to peak flow, MoTI supported the Pacific Climate Impacts Consortium (PCIC) in a pilot project to estimate historical and future design flow values for the upper Fraser watershed, a 34200 km^2 section of the Fraser River basin upstream of Prince George, BC (Schoeneberg et al., 2021). Historic and future streamflow used results derived from VIC-GL hydrologic projections forced with the CanESM2 50-member initial-conditions ensemble (CanESM2-LE). These design flood values were estimated on the 0.0625° x 0.0625° VIC-GL computational grid and were provided as a prototype online design flow tool that has been integrated into the PCIC Climate Explorer. Following a review by MoTI staff, PCIC was asked to revise and upgrade the tool, including expanding the study domain to include the entire Fraser basin, provide design flow estimates as a ratio of future value to historic value, provide changes factors at 10-year intervals using a 30-year sliding window, centered on 2015, 2025, 2035, 2045, 2055, 2065, 2075, and 2085 based on CanESM2 Large Ensemble with RCP8.5 (Schnorbus and Sun, 2022)[1]. PCIC has subsequently been tasked by MoTI to further revise and upgrade the tool as follows:

1. Data Products and Analysis: Expand the study domain to provide gridded design flow estimates for the Peace River basin upstream of Peace River, AB, and complete the hydrologic projections needed for future extension of gridded design flow estimates into the upper Columbia; and
2. Tool Updates: Address items in the online tool interface identified as bugs, UI improvements, and missing data.

As discussed in Schnorbus and Sun (2022), VIC-GL streamflow simulation in the Chilcotin sub-basin was very poor. Therefore, additional work was conducted as part of the Data Products and Analysis work to generate updated projections and gridded design flow values for the Chilcotin basin as well.

The 'Data Products and Analysis' work again takes advantage of hydrologic projections produced by PCIC using the VIC-GL hydrology model driven with the CanESM2 50-member large ensemble (CanESM2-LE) (Government of Canada, 2019; Kushner et al., 2018). This large ensemble (7500 simulation years), which is based on the RCP8.5 scenario, provides sufficient peak flow samples to allow statistically robust estimation of large return-period events. The use of large-ensembles as a means to develop robust projections of changes to climate extremes and flood frequencies is well established (Ben Alaya et al., 2020; Curry et al., 2019; Fyfe et al., 2017; Gao et al., 2020; Kirchmeier-Young et al., 2017b; Kirchmeier-Young and Zhang, 2020; Li et al., 2019, 2020).

[1] https://services.pacificclimate.org/pcex/app/#/data/flood/fraser

The following items have been delivered as part of this project:

1. Hydrologic projections for the Peace and upper Columbia basins based on the CanESM2 50-member large ensemble using the RCP8.5 emissions scenario. Large ensemble projections have now been completed on a domain covering 665,000 km^2.
2. Gridded design flow values and change factors for 2-, 5-, 10-, 20-, 50-, 100-, and 200-year events for the Peace River basin for a combined domain spanning 414,000 km^2,
3. Updated streamflow projections and gridded design flow values and change factors for the Chilcotin basin
4. Tool updates and improvements.

The purpose of this report is to describe the tool updates and to provide the necessary background in support of the expanded Data Products and Analysis component of the project. Section 2 of the report describes the updates the PCEX Extreme Streamflow Tool. The remainder of the report, Sections 3 through 6, describes the Data Products and Analysis component of the project and is structured as follows. Section 3 describes the study area, section 4 details the methodology of the hydrologic model and its parameterization, the CanESM2 Large Ensemble (LE), the downscaling method, the flood frequency analysis and summarize the overall study design. Results are presented in section 5, and discussion of model results, uncertainties and limitations is covered in Section 6. Conclusions are presented in Section 7.

2 Tool Updates

Based on user feedback, a number of improvements have been implemented to the Extreme Streamflow User Interface (UI) of the PCIC Climate Explorer (see https://services.pacificclimate.org/pcex/app/#/data/flood/fraser). These improvements are detailed in Table 1. In addition, gridded design flow values and change factors for the Peace basin have also been uploaded and are now accessible via the Extreme Streamflow UI.

Table 1. Tool User Interface Improvements

Issue	Explanation	Resolution
Tried importing a shape file: After importing the shaped zipped file, it gave an error in the attribute table (right bottom) – Error: 400 received from data server	I suspect the tool does not 'know' how to find the outlet when an arbitrary watershed boundary is imported and, therefore, cannot estimate any 'upstream' information.	The "import Polygon" feature has been removed from the map interface to avoid confusion
I couldn't get the "create polygon" feature work for the streamflow	There is not a "create polygon" tool for streamflow, because we can only provide streamflow at a point (outlet). The tooltip is named "Draw a circlemarker", so we will re-label this to "Select an outlet"?	This is strongly tied to the underlying tool library and not easily fixable. The tooltip is still named "Draw a circlemarker", but the 'Data Map' help has been updated to describe the tool's purpose as selecting an outlet location.
When you flip between different scenarios 2-year annual max to 100-year annual max. It changes the graph and AS colors but no feedback that it is showing the results of the watershed or your point of interest. I am pretty sure it is but there is no feedback or intuitive. Maybe I can explain better in a demo	When an outlet location is selected on the map the graph shows results at the outlet point and table summarizes watershed characteristics upstream of the outlet point. Results are not averaged over grid cells. The polygon on the map is meant to show the upstream region corresponding to the selected outlet point.	Changed the 'Data Graphs and 'Design Values' context help to explain the source of the data values.
What is rXi1p1? Would be nice if it is defined somewhere.	When individual ensemble members are displayed this makes sense (i.e., r2i1p1). However, as we group all ensemble members together from a single GCM, the label is meant to convey that the data derives from a pooling together of multiple ensemble members for each period (r1 + r2 + r3 + … + r10 = rX).	An explanation has been added to the 'Filtered Datasets Summary' tool help.

Issue	Explanation	Resolution
Why do we have only mean for 200 years whereas for all other return periods, we have 97.5%, mean and 2.5%?	Need to add confidence bounds to cfrp200 (aClim_9750P and aClim_0275P)	Generated and added missing data
The map tools need to more self-explanatory, and the map should emphasize the screen space. For example, the tool "Draw a circlemarker" does not indicate that it is delineating a watershed. "Target location" or "Watershed delineation" would be more suitable descriptors.	Better tool documentation is required.	Tool documentation has been updated.
The slide bar for the climate raster layer can be a bit glitchy in that it can also grab the map when you try to change the opacity.	Noted.	Issue could not be resolved as this is a bug in the underlying leaflet tool library.

3 Study Area

For this project, the spatial domain was expanded to include the Fraser basin, the Peace River basin above Peace River, AB, and the upper Columbia River above the Priest Rapids Dam[2], for a combined drainage area of 665,000 km^2. (Figure 1). Based on PNWNAmet (Werner et al., 2019) the 1981-2000 mean annual temperature for the three basins combined is 1.0 °C. Mean annual temperature ranges from a low of < -4 °C at high elevations in the Coast and Columbia Mountains (Fraser and upper Columbia) and the Cassiar Mountains (northern Peace basin), to a high of 10-11 °C in the low-lying Fraser River delta and southern Columbia (Figure 2). Due to the complex topography, precipitation in the basin exhibits high spatial variability (Figure 3). Annual precipitation is highest along the windward length of the Coast Mountains in the lower Fraser, with a secondary wet band along the Rocky and Columbia Mountain in the headwaters of the Fraser, Columbia, and Peace basins. Due to a heavy rain shadow effect, precipitation decreases dramatically in the interior of the Fraser and Columbia and east of the Rockies in the Peace. Precipitation is highest (> 4000 mm) along the windward-facing North Shore Mountains at the basin outlet, and lowest (< 300 mm) in the central interior.

For presentation purposes (see Sections 5.2), the Peace basin has been divided into seven sub-basins that are delineated based on the locations of Water Survey of Canada gauges and BC Hydro project sites. The characteristics of these sub-basins are summarized in Table 2 and shown in Figure 1. The Finlay River sub basin (FRAAR) delineates the northern headwaters of the Peace basin, draining the Cassiar and Northern Rocky Mountains into the norther end of the Williston Reservoir. The Nation River (NRNTM) is a relatively small sub basin that drains the Cassiar Mountains eastward into the Williston Reservoir. The Peace River at Bennet Dam (PRABD) delineates the entire drainage area upstream of the dam (including FRAAR and NRNTM) and encompasses the western half of the Peace basin domain, receiving runoff from both the Cassiar and northern Rocky Mountains. The W.A.C. Bennett Dam, which forms the Williston Lake Reservoir, the largest lake in British Columbia, regulates discharge at the outlet of PRABD and, consequently, flow throughout the entire main stem of the Peace River below PRABD is also regulated. The Pine River (PRAEP), an unregulated tributary of the Peace, drains the leeward side of the Northern Rock Mountains and flows east into the Peace River main stem below the Bennett Dam. The Beatton River (BRNFS), a tributary that drains south into the Peace River, is located entirely on the Interior Plains east of the Rocky Mountains and, as such, has considerably lower relief than the other sub basins. The Smoky River (SMRAW) rises along the leeward side of the Rocky Mountains and flows east through the plains into the Peace River just upstream of Peace River, AB. Although most of the SMRAW is located on the plains, the headwaters contain some of the highest elevations in the Peace basin domain. Although some sub-basins contain glacier coverage (FRAAR, PRABD, PRAEP, and SWRAW; Table 2), relative coverage in all cases is negligible (< 0.1%). The Peace River at Peace River (PRAPR) denotes the outlet of the entire Peace River domain. The flow at this location is regulated due to the presence of the W.A.C. Bennett dam. Note that simulated streamflow represents natural flows that do not account for flow regulation (see Section 4.5).

The mean annual temperatures of the Peace basin are quite low (Table 2), consistent with its high-latitude continental location. There is some variation in temperature between the sub basins that is generally correlated with median basin elevation, ranging from -1.3 °C in FRAAR (1484 m) to 2.1°C in SWRAW (871 m). The is a west-to-east precipitation gradient in the Peace basin (Figure 3) is also reflected in the mean sub basin values, which tends to be higher for western sub-basins that drain the Cassiar and Rocky

[2] https://en.wikipedia.org/wiki/Priest_Rapids_Dam

Mountains (FRAAR, NRNTM, PRABD, and PRAEP and lowest for eastern sub-basins located predominantly on the Interior Plains (BRNFS, SWRAW, and PRAPR)

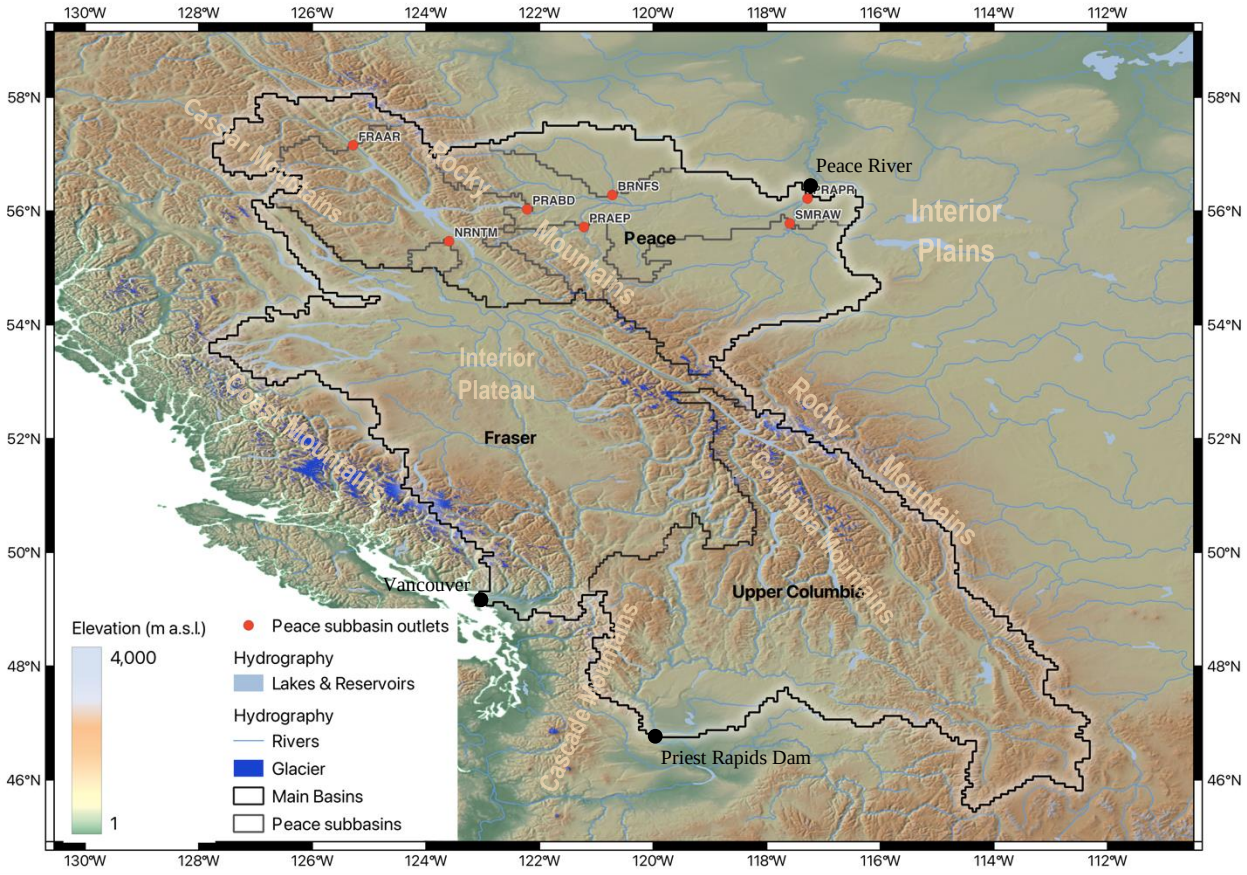

Figure 1. Project domain showing the upper Columbia basin above Priest Rapids Dam, the Fraser basin above tidewater at Vancouver, and the Peace basin above Peace River, AB. Also shown are subbasin outlines and outlet points for the Peace River basin. Large ensemble hydrologic projections have been generated for all three basins, but gridded design flow values are only available for the Peace and Fraser basins.

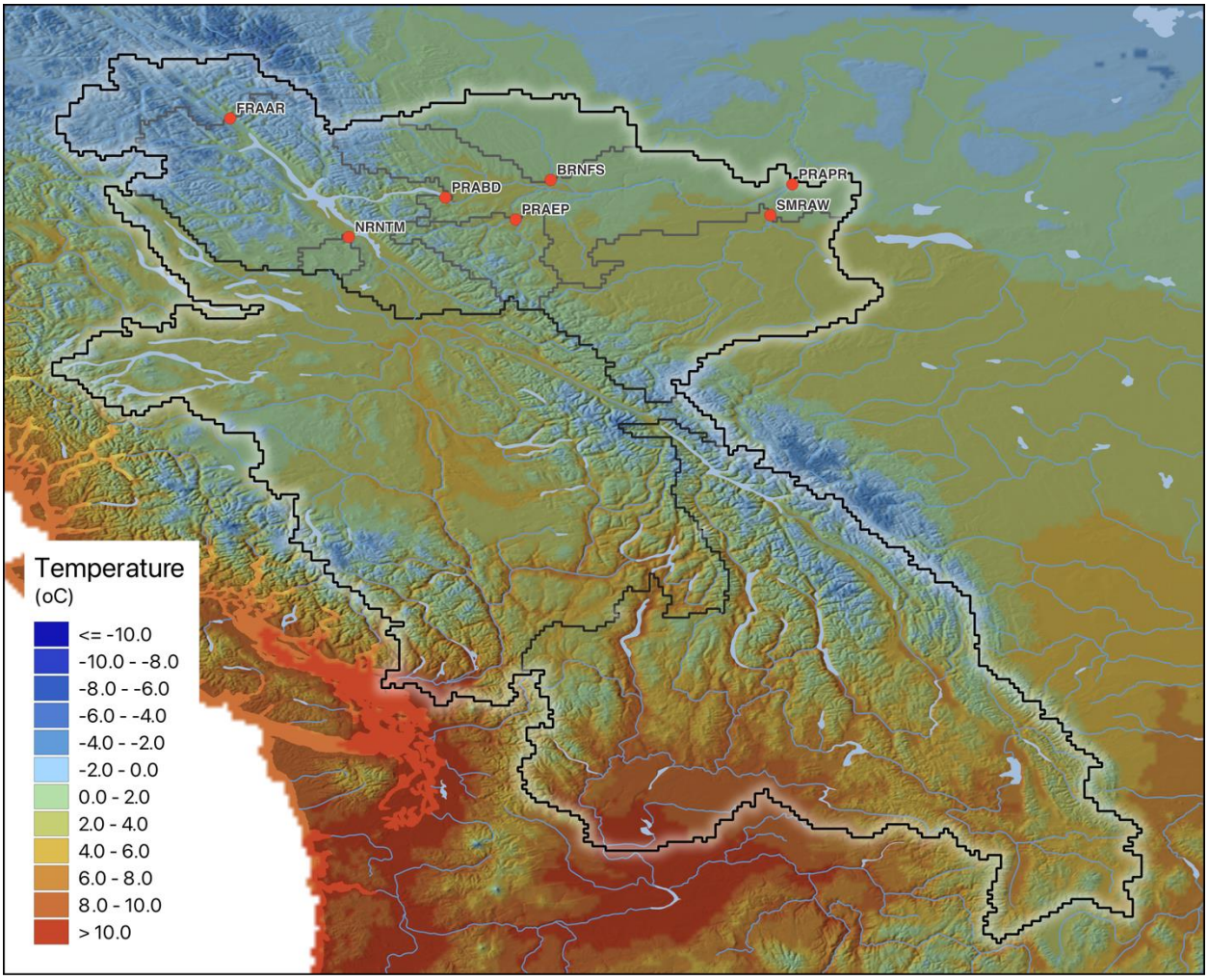

Figure 2. Annual average temperature for 1980-2010 from PNWNAmet.

Table 2. Sub-basins of the Peace

Basin Code	Basin Name	Area (km^2)	Glacier Area (km^2)	Elev. Min (m)	Elev. Median (m)	Elev. Max (m)	Temp. Mean (°C)	Pr. Mean (mm/a)
FRAAR	Finlay River above Akie River	15600	171	691	1484	2685	-1.3	770
NRNTM	Nation River near the Mouth	2500	0	737	1024	1515	1.1	800
PRABD	Peace River at Bennett Dam	76400	203	594	1279	2685	-0.1	800
PRAEP	Pine River at East Pine	12100	13	539	1115	2330	1.2	950
BRNFS	Beatton River near Fort St. John	15600	0	481	780	1666	1.1	480
SMRAW	Smoky River at Watino	50300	181	369	871	2980	2.1	660
PRAPR	Peace River at Peace River, AB	203940	469	289	956	2980	1.0	690

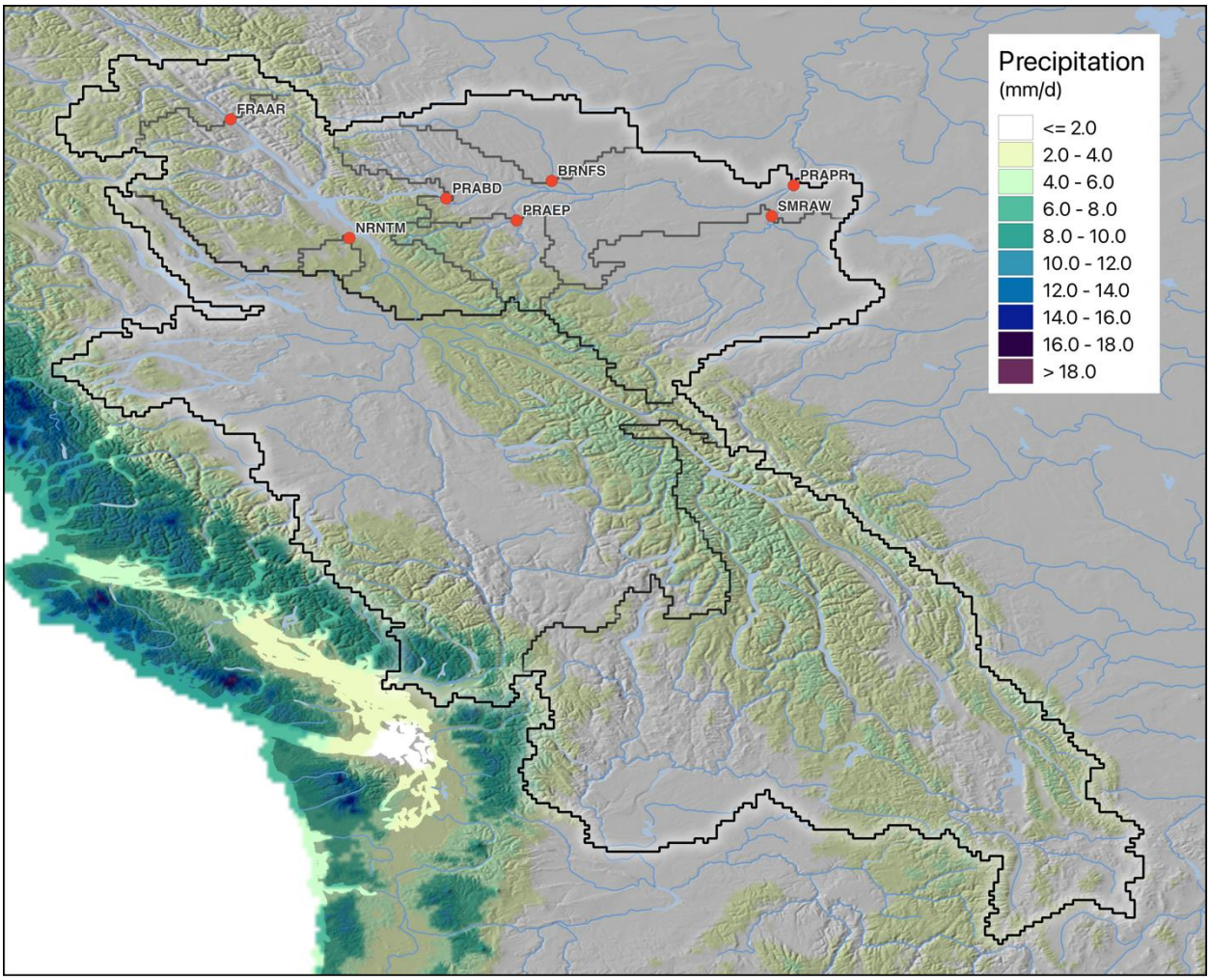

Figure 3. Annual average precipitation for 1980-2010 from PNWNAmet.

4 Models and Methodology

The method for producing the data products remains the same as that used in the pilot study. Namely, empirical frequency analysis was performed on daily streamflow simulated using the VIC-GL model driven by the CanESM2 Large Ensemble, which was forced with the RCP8.5 scenario. The analysis was performed on a cell-by-cell basis on the VIC-GL computational grid for the entire proposed domain. The projections of future annual maximum streamflow and their flood frequencies requires a chain of models. The following provides details on each modelling component and summarizes the overall study design. A graphical summary of the study design is given in Figure 4. The implications of the chosen design with respect to modelling uncertainty and limitations will be discussed in Section 6.

4.1 CanESM2 – Large Ensemble

Future climate projections at the regional scale start with model simulations of the global climate system. Because these are models, there is inherent uncertainty related to (1) the assumptions about how the greenhouse gases (GHG) will evolve, (2) the climate model and how it represents the physical processes and (3) the internal variability, e.g. the natural variability that we experience as weather or El Nino events, which is irreducible (Arora and Cannon, 2018; Cannon et al., 2020). The hydrologic projections were produced using climate simulations from CanESM2, which is a coupled Earth system model developed and run by the Canadian Centre for Climate Modelling and Analysis (Arora et al., 2011). CanESM2 is part of the World Climate Research Programs (WCRP) fifth Coupled Model Inter-comparison Project (CMIP5) (Taylor et al., 2011). The CMIP5 submission of CanESM2 included five ensemble members run with historical forcings from 1850 to 2005. A much larger ensemble of climate projections was produced by expanding the ensemble to 50 members, each spanning the period 1950 to 2100 (Government of Canada, 2019; Kirchmeier-Young et al., 2017a; Kushner et al., 2018). A random number generator with a pre-set seed was used to perturb slightly the initial state of each of the 50 ensemble members. Thereby, quasi-independent climate change realizations were generated without any change to the model dynamics, physics or structure (Fyfe et al., 2017). The resulting ensemble represents 50 equally plausible realizations of the evolution of the global weather and climate that are consistent with the observed emissions over the period 1950 to 2005 and the RCP 8.5 emissions scenario from 2006 to 2100. In the RCP8.5 scenario, emissions continue to rise throughout the 21st century and this scenario is often used as the basis for worst case climate change.

4.2 Downscaling

The climate response to a prescribed RCP scenario that is obtained from a climate model is of too coarse a spatial resolution, with individual grid cells typically encompassing 10,000 km^2, to be used directly in driving a hydrology model. For example, GCM output at this resolution does not reflect the detailed spatial variation in climate due to local orography and variations in land surface properties that are necessary for simulating surface hydrology well. Therefore, to model changing hydrologic conditions at local and regional scales, daily values of minimum temperature, maximum temperature and precipitation have been statistically downscaled to the resolution of VIC-GL. This downscaling used the Bias Correction/Constructed Analogues with de-trended Quantile mapping reordering downscaling technique (BCCAQv2) (Hiebert et al., 2018) with PNWNAmet (Werner et al., 2019) as the reference meteorology. BCCAQv2 is a hybrid method that combines results from bias-corrected constructed analogs (BCCA) (Maurer et al., 2010) and de-trended quantile mapping (QMAP) (Gudmundsson et al., 2012). BCCA obtains spatial information from a linear combination of historical analogues for daily large-scale fields. QMAP applies quantile mapping to daily climate model outputs interpolated to the high-resolution grid using the climate imprint method of Hunter and Meentemeyer (2005). The BCCAQv2 method includes a revision to the quantile mapping procedure that better preserve changes in quantiles and extremes

(Cannon et al., 2015) as compared to its original implementation. BCCAQv2 works well for hydrologic extremes because of its ability to resolve event-scale spatial gradients (Werner and Cannon, 2016). For more information on BCCAQv2 see (Cannon et al., 2015; Hiebert et al., 2018; Sobie and Murdock, 2017; Werner and Cannon, 2016).

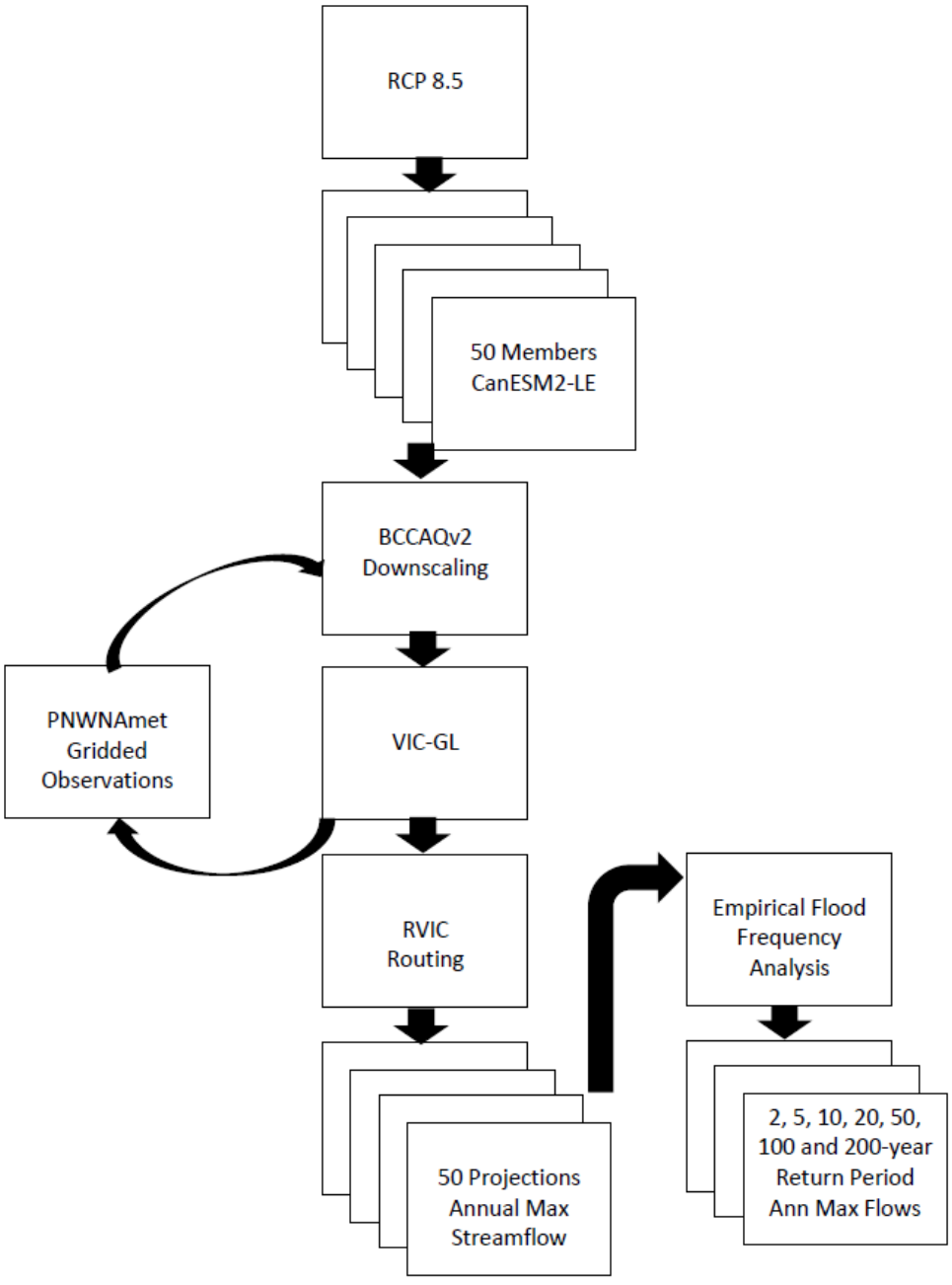

Figure 4. Modelling workflow used to derive estimates of annual maximum streamflow quantiles from the CanESM2 large ensemble.

4.3 VIC-GL Model Summary

Streamflow was simulated with VIC-GL, an upgraded version of the Variable Infiltration Capacity (VIC) model that explicitly models glacier mass balance (accumulation, melt and runoff) and glacier dynamics (change in glacier area) (see Schnorbus 2018 for details). VIC is a spatially distributed macro-scale hydrologic model that calculates water and energy balances in each grid cell. Spatial variability in soil properties within a drainage basin is modelled by sub-dividing the model domain into a computational grid with a spatial resolution of 0.0625° latitude by 0.0625° longitude (approximately 6 km x 5 km within the study region). The variability of land cover and topography within individual grid cells is further described using hydrologic response units (HRUs) which characterize land surface properties as a function of elevation. VIC runs at a 3-hour temporal resolution and output is aggregated to daily values. Soil moisture processes are represented by three-soil layers, spatial heterogeneity of runoff generation with variable infiltration curves, and subsurface flow generation using the Arno conceptual model (Todini, 1996). Surface runoff is generated when the moisture exceeds the storage capacity of the soil. Water fluxes are computed for a range of hydrologic processes such as evapotranspiration, snow accumulation, snowmelt, infiltration, soil moisture and surface and subsurface runoff. A detailed description of the baseline VIC model is available in Liang et al. (1996, 1994) and Cherkauer et al. (2003).

VIC-GL uses several parametrization strategies to describe the influence of topography and vegetation cover. Sub-grid elevation is described using 200-m elevation bands derived from the GMTED2010 digital elevation model (Danielson and Gesch, 2011). Vegetation classification utilizes the North America Land Cover dataset, edition 2 (Natural Resources Canada / The Canada Centre for Mapping and Earth Observation 2013) produced as part of the North America Land Change Monitoring System (NALCMS). The NALCMS land cover data set divides North America into 19 classes representing circa 2005 conditions, with most forest areas in the region for which VIC-GL has been parameterized being included in a single class, the temperate or sub-polar needle-leaf forest class. This homogeneous region has therefore been further subdivided based on vegetation height and leaf area index. Leaf are index data is from the GEOV1 global time series dataset (Baret et al., 2013; Camacho et al., 2013). Vegetation height is based on global mapping using space borne light detection and ranging (LIDAR) (Simard et al., 2011). The final land cover classification, with needle-leaf forest further sub-divided, contains 22 land cover classes. Although an Ice class exists in the NALCMS-based land cover inventory, the extent and location of glaciers and ice fields was updated using the Randolph Glacier Inventory (RGI) version 3.2 (Pfeffer et al., 2014). Soil classification and parameterization relies on physical soil data from the Soils Program in the Global Soil Data Products CD-ROM (Global Soil Data Task, 2014).

Calibration is the process whereby certain model parameters are adjusted such that simulated output is in close agreement with observations. During the calibration process, VIC-GL was forced with the PNWNAmet gridded meteorological data set (Werner et al., 2019). Model calibration used a multi-objective approach that constrained the model using observations of streamflow, evaporation, snow cover and glacier mass balance (estimated from thinning rates). For more details on calibration process, see Schnorbus (2017). An evaluation of VICGL overall performance for the Peace and Fraser is reported in Schnorbus (2021) and direct verification of simulated annual maximum streamflow for the Peace basin is provided as Appendix A.

4.4 Surface Routing

Surface water routing is applied as a post-processing step in the modelling chain using the RVIC model (https://rvic.readthedocs.io/en/latest/), which is based on the numerical schemes described in Lohmann et al. (1998). Note that streamflow simulated by the VICGL-RVIC models only represents natural flows.

Hence the results will not reflect the effects of flow regulation in those portions of the Peace, Fraser and upper Columbia that are affected by reservoir storage and releases. A two-step process is used to rout runoff and baseflow generated in each VIC-GL model cell: in-grid routing and channel routing. In-grid routing conceptually moves surface runoff through the sub-grid drainage network to the main channel using a transfer function that essentially describes the time distribution for runoff reaching the outlet of a grid box. The transport of water within the channel is modelled using a one-dimensional diffusive wave approximation to the full Saint Venant equations. The channel system is defined by assigning one of eight flow directions (N, NE, E, SE, S, SW, W or NW) to each cell. The resultant channel network and flow accumulation (the number of upstream cells) for all three main basins in the study area is shown in Figure 5.

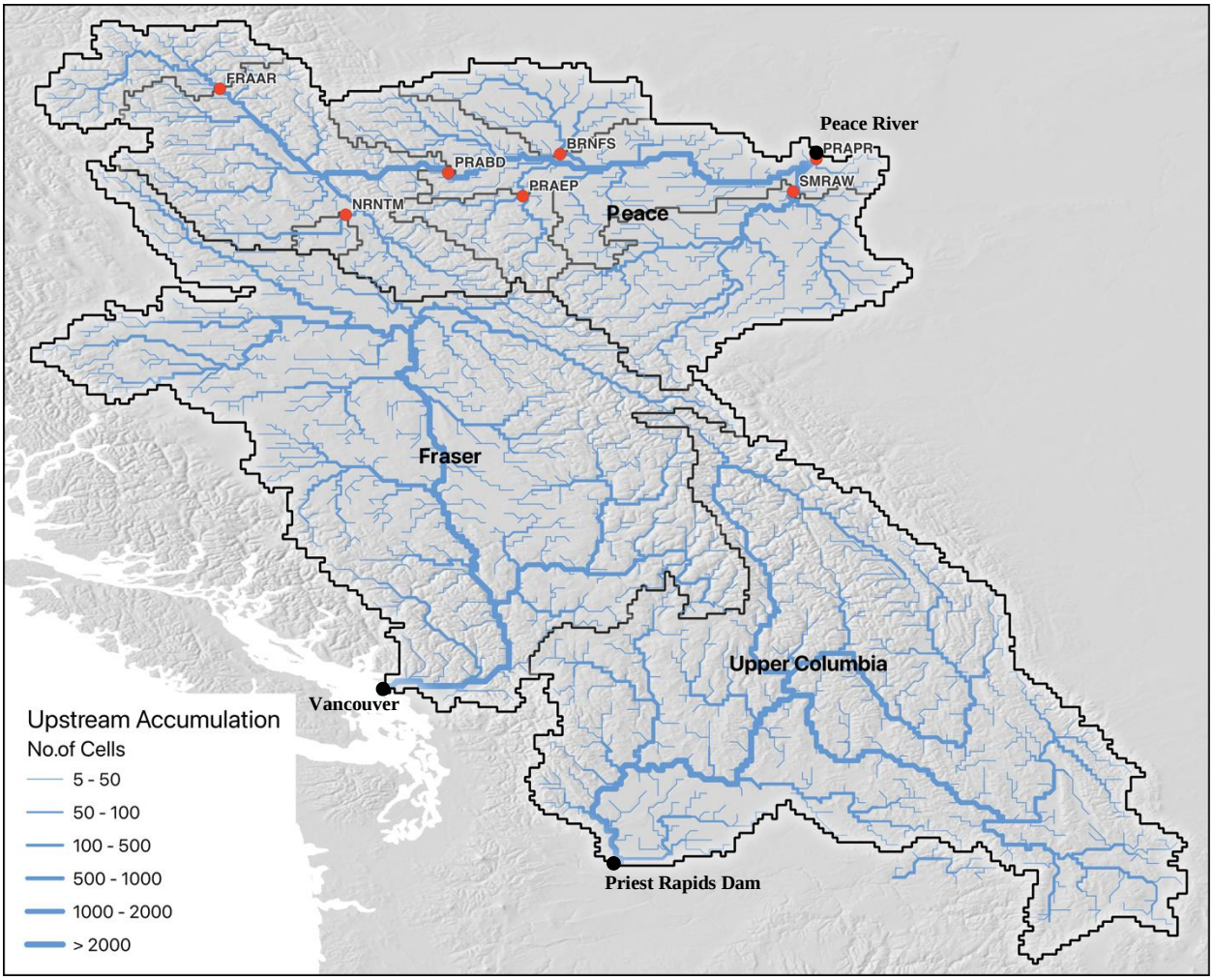

Figure 5. VICGL flow network for the upper Columbia, Fraser, and Peace with flow accumulation (as the number of upstream cells). Also shown are sub-basins and outlet points for the Peace. The flow threshold has been set to five grid cells (i.e. channels with upstream flow accumulation less than five cells are excluded from the image).

In-grid routing is parametrized by specifying the unit hydrograph for each grid cell. Channel routing requires specification of the channel length, wave celerity and diffusivity for each grid cell. Based on

manual calibration, wave celerity is assumed constant at 2.0 m/s and channel diffusivity is set to 1300 m. Channel length is estimated as the cell height and cell width for north-south, east-west flow directions, respectively, and as the cell diagonal for all remaining flow direction.

4.5 Flood Frequency Analysis

The design of roads, bridges, culverts, and other structures often requires estimates of peak flow quantiles that correspond to return periods varying from 2-years up to perhaps 200-years, depending on the application. When reliant on small sample sizes to estimate peak flow quantiles, as is typically the case when using observed data, these quantiles often correspond to return periods that are substantially longer than the sample. In these cases, one must generally resort to parametric flood frequency approaches so that one can extrapolate beyond the data to produce the necessary quantile estimates, such as using the Generalized Extreme Value, or GEV, distribution to describe the available peak flow data. Unfortunately, parametric approaches may suffer from some lack-of-fit that can result in biased quantile estimates, particularly for infrequent events. The benefit of using the CanESM2 large ensemble is that it provides enough samples of identically distributed annual maximum events that the quantiles, even for very large design values such as the 200-year event, can be estimated directly from the empirical cumulative distribution. For this project it was determined that hydrologic projections for five ensemble members could not be used due to incomplete spatial coverage. Hence, only 45 ensemble members were used in subsequent analysis.

Streamflow extremes were analyzed at ten-year intervals using a 30-year sliding window centered on 2015 (2001- 2030), 2025 (2011-2040), 2035 (2021-2050), 2045 (2031-2060), 2055 (2041- 2070), 2065 (2051-2080), 2075 (2061-2090), and 2085 (2071-2100). Annual maxima were extracted for each year and pooled across model runs of the large ensemble, resulting in 1350 values for each thirty-year period (30 years by 45 ensemble members) from streamflow simulated at each grid point. Quantiles were estimated empirically using the function “quantile” from the R stats package (R Core Team, 2019). We used the default quantile algorithm where the p^{th} percentile from the sample is estimated as:

$$x_{\lfloor h \rfloor} + (h - \lfloor h \rfloor) \times (x_{\lceil h \rceil} - x_{\lfloor h \rfloor}) \quad (1)$$

where $h = (N - 1)p + 1$ and N is the number of samples. Note that for very high quantiles, empirical estimates can be somewhat biased depending on the choice of plotting position formula. However, because 200-year return levels (99.5 percentiles) are estimated from 1350 years of data we don’t consider this as a point of concern. We estimate the 50th, 80th, 90th, 95th, 98th, 99th, and 99.5th percentile of the 1350 samples, which corresponds to the 2-, 5-, 10-, 20-, 50-, 100- and 200-year return levels, respectively. We define the median quantile estimates as those derived from the full sample. The confidence intervals for each quantile are quantified using the following bootstrapping approach: (1) for each 30-year block randomly sample with replacement a sample of size n=1350 from the pooled results across all 45 ensemble members; (2) estimate the quantiles from the new sample using equation 1; (3) repeat steps (1) and (2) 1000 times, and (4) estimate the 2.5% and 97.5% percentiles from the 1000 quantile estimates at each return level to obtain the 95% confidence intervals.

Projections of change were assessed by converting the absolute streamflow design values into change factors. Change factors are the ratio of future value to baseline value. Change factors utilize a baseline period of 1951-2000. This means that the quantiles for the baseline period are estimated from samples of size 50x45 = 2250 years. The confidence intervals for each quantile are estimated in a similar bootstrapping fashion as the underlying quantiles using the following approach: (1) for each 30-year

block randomly sample with replacement a sample of size n=1350 from the values pooled across all ensemble members; (2) randomly sample with replacement 45 years across all ensemble members from the baseline period for sample of size n=2250; (3) estimate quantiles from each thirty-year block and the baseline block and calculate change factor for each quantile; (4) repeat steps (1), (2), and (3) 1000 times; and (5) estimate the 2.5% and 97.5% change factor percentiles from the 1000 change factor estimates at each return level to obtain the 95% confidence intervals. As the change factor is a ratio of two random variables, this approach explicitly considers the underlying sampling variability of both quantiles (future and baseline) when estimating the uncertainly of the change factors.

5 Results

5.1 Spatial Pattern of Projected Changes in Peak Flow

We describe the projected changes in design flood values at each individual grid cell in the Fraser and Peace domains. Note that these figures incorporate the updated projections for the Chilcotin basin (see Section 5.3). Change factors for the 2-year and 100-year events are displayed in Figure 6 and Figure 7, respectively. Specific runoff (runoff/unit area) is higher in wetter climates than it is in drier climates, so for an equal size drainage area, wetter climates produce larger magnitude flood events. Therefore, at the local scale (about 100 km^2), the spatial distribution of peak flow magnitude is broadly consistent with precipitation climatology (Figure 3). However, as runoff is integrated over increasingly larger scales, peak flow magnitude in larger basins tends also to increase with increasing drainage area. Consistent with the topology depicted in Figure 5, the largest peak flow values occur where flow concentrates along major tributaries and the main stem of the Fraser and Peace Rivers. The result is that flow design values span several orders of magnitude across the basin. For example, the 2-year design event ranges from <1.0 m^3/s for headwater cells in the drier interior regions to over 9000 m^3/s and 14000 m^3/s at the outlets of the Peace and Fraser, respectively (Figure 6). For the 100-year event the range is <1.0 m^3/s to over 13000 m^3/s and 17000 m^3/s at the outlets of the Peace and Fraser, respectively.

Changes in peak flow magnitude at each grid cell will be influenced by numerous factors, the relative importance of which vary as a function of spatial scale. For cells draining very small drainage areas, individual grid cell changes will be affected more by local elevation, relief, and changes to the local climate, whereas peak flow changes in cells draining larger areas are likely influenced by changes occurring in distant (potentially wetter) upstream locations. Consequently, at the individual cell scale the spatial patterns of peak flow change for the 2- and 100-year events displays a rather heterogeneous pattern, without a clear widespread relationship to either topography, climate, or network topology (Figure 6 and Figure 7, respectively). Spatial heterogeneity is also affected by noise resulting from model error and calibration artifacts. Model uncertainty is discussed in detail in Section 6.

Basin-wide, however, there broad trends that emerge. For the 2-year event, the projected mean change factors over the basin show a mixed response at mid-century (2041-2070), where both increases and decreases in peak flow are projected in the Fraser but predominantly increasing flows are projected in the Peace (Figure 6). At end-century (2071-2100, the response throughout most the Fraser shows 2-year design flows decreasing below baseline levels, although there are some regions (such as the lower Fraser Valley near the outlet) where flows are projected to increase. At end-century in the Peace the 2-year design flow is projected to increase throughout most of the basin. For both basins the magnitude of the change, whether increase or decrease, tends to be larger at end-century than at mid-century.

For the 100-year event in the Fraser most grid cells exhibit increases during mid-century, but by end-century a larger number of grid locations will see design flow values decrease below baseline values (Figure 7). In contrast, most of the Peace basin is expected to experience increasing design flow magnitudes at both mid- and end-century.

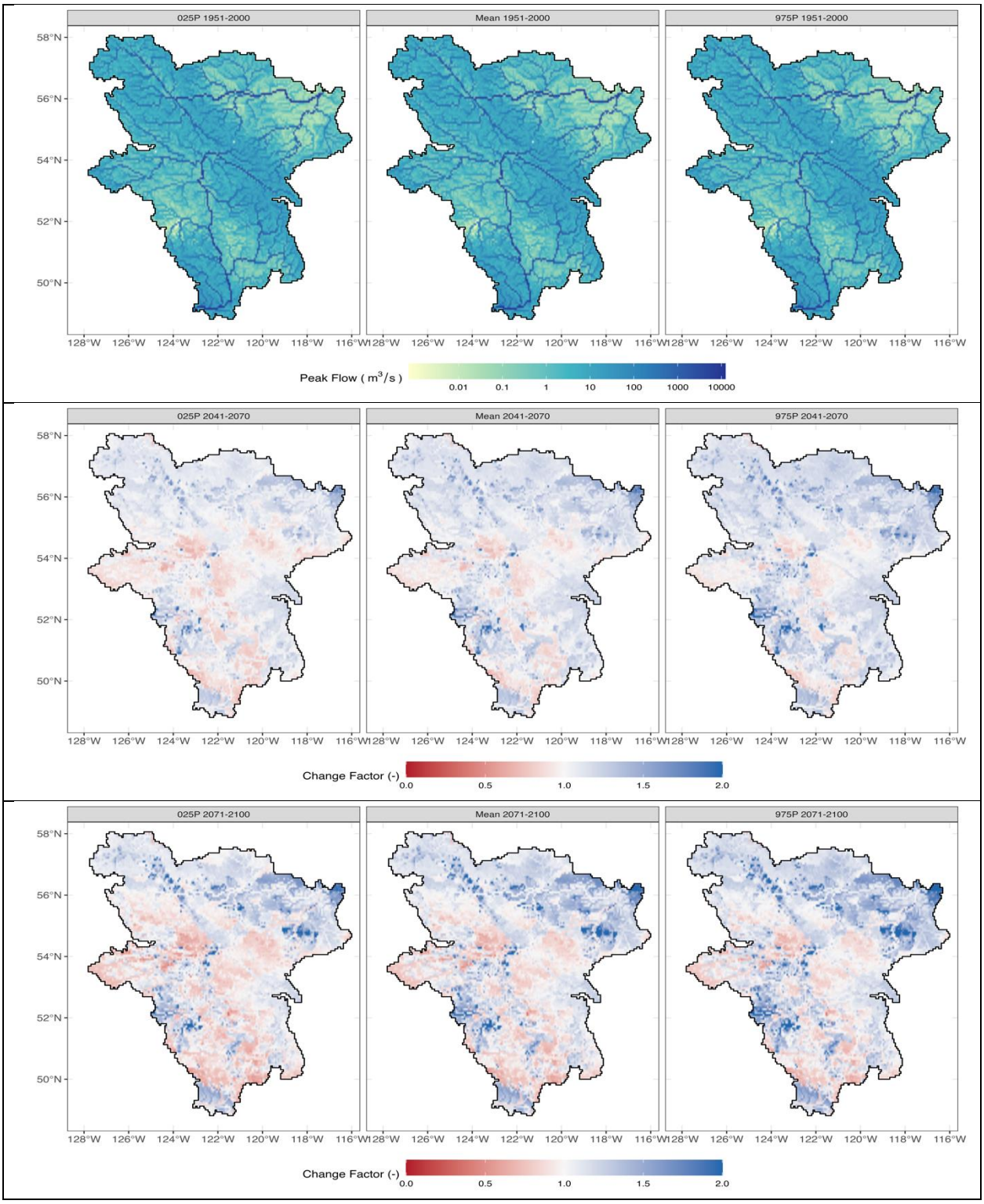

Figure 6. The absolute value (m^3/s) of annual peak flow during the 1951-2000 period (plotted on logarithmic scale) (top) and change factors in annual peak flow magnitude for 2-yr return period events for 2041-2070 and 2071-2100 versus the baseline period (1951-2000). Results are shown for 2.5th percentile (left), median (middle) and 97.5th percentile (right).

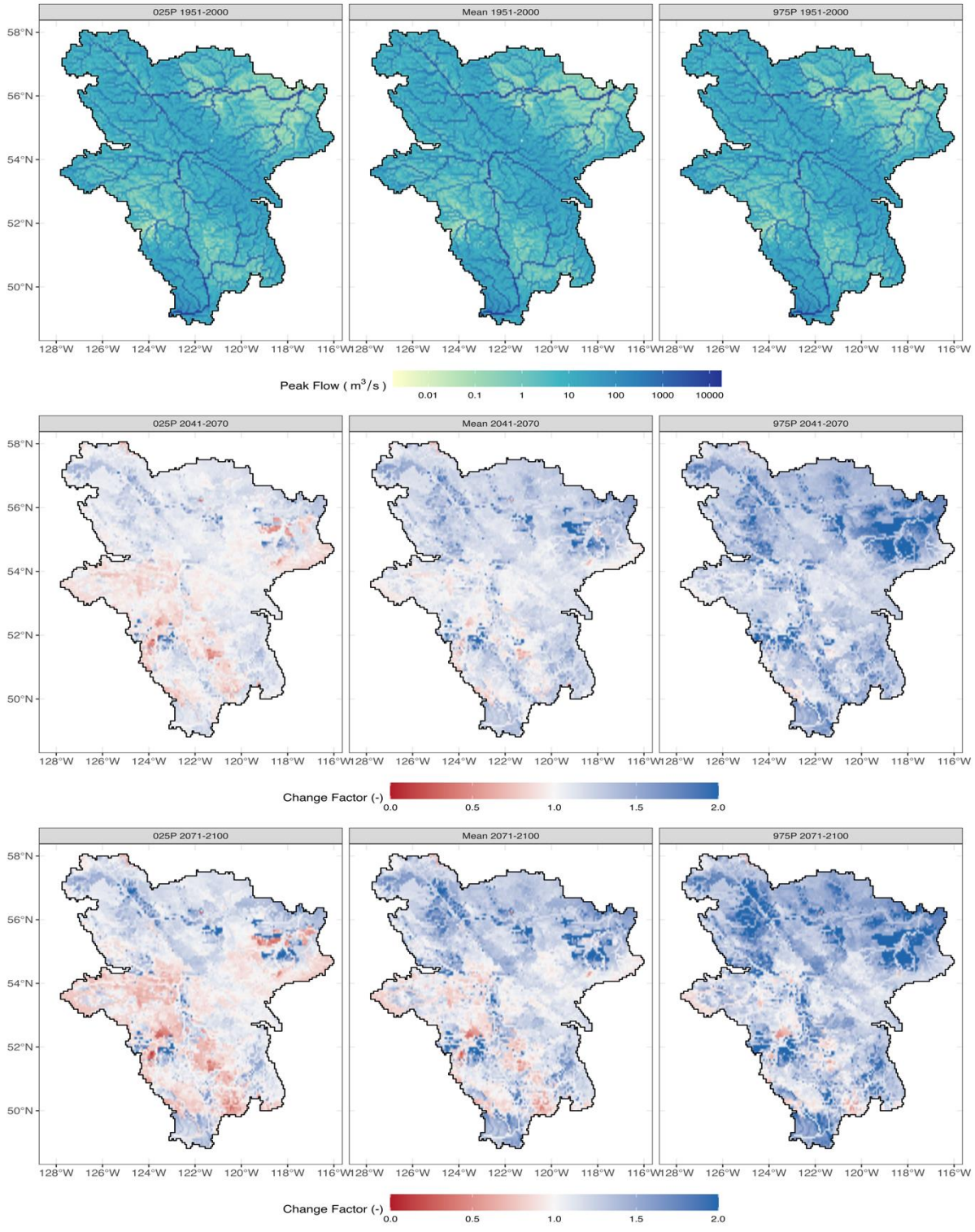

Figure 7. The absolute value (m^3/s) of annual peak flow during the 1951-2000 period (plotted on logarithmic scale) (top) and change factors in annual peak flow magnitude for 100-yr return period events for 2041-2070 and 2071-2100 versus the baseline period (1951-2000). Results are shown for 2.5th percentile (left), median (middle) and 97.5th percentile (right).

5.2 Projected Changes in Peak Flow by Sub-basin

In this section we focus on results for the newly added Peace River basin. Results for the Fraser basin are reported in Schnorbus and Sun (2022). We present the flood frequency results for six locations corresponding to the outlets of the FRAAR, NRNTM, PRABD, PRAEP, BRNFS, and SMRAW as well as the outlet of the Peace River basin (PRAPR). Results are summarized graphically as flood frequency curves (Figure 8) and corresponding change factors (Figure 9) for select return periods. When design flood is plotted versus return period, results indicate that the projected flood frequency response to climate change in the Peace varies by sub-basin and period (Figure 8). All sub-basins project an increase in flood magnitude during the early century period (2011-2041) for all return periods (excepting PRPAR for the 200-year event). At mid-century (2041-2017) flood magnitudes are either larger (FRAAR, NRNTM), or generally similar (BRNFS, PRABD, PRAEP, SMRAW) than at early-century. The greatest variability between basins tends to occur during end-century (2071-2100). In basins such as BRNFS and FRAAR, flood magnitude is projected to continue increasing beyond mid-century levels for all return periods. In other basins (e.g., NRNTM, PRABD, PRAEP, and PRAPR) flood magnitude will continue increasing for large return period events (T > 20 - 50 years) but will decrease below early-century levels for small return period events. In one case (SMRAW), flood magnitude for small events (T < 50 years) are projected to decrease below baseline magnitudes.

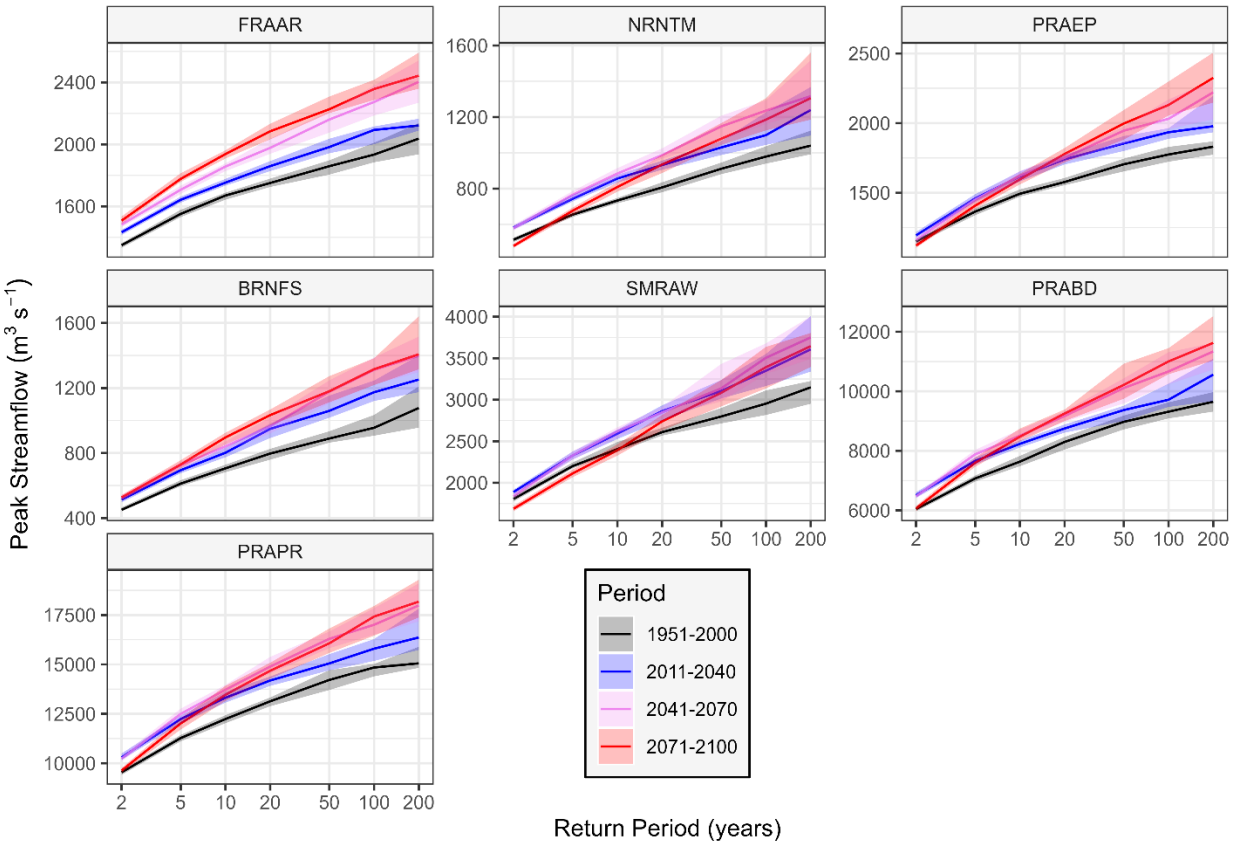

Figure 8. Plot of design streamflow versus return period for four periods at the outlets of six sub-basins and the Peace River basin. The median is given by the solid line and the ribbon shows the 95% confidence interval.

In Figure 9, change factors for select return periods are plotted as a function of future period, where we note that time is also a proxy for increasing climate warming. At all sites the change factors tend to start above one, reflecting the change between the reference period (c. 1970s) and the first 30-year period (2001-2030). We also note the variability of the climate change response between sub basins different design levels. For the 2-year event the peak flow response is generally non-monotonic (not constantly increasing or decreasing) with increasing time, where flow magnitude increases until around mid-century, at which point it is expected to decline. In certain sub basins the magnitude of the 2-year event is expected to be less than the baseline value by end-century. The timing of the inflection point between increasing and decreasing flow, and the time at which flow decreases below baseline, varies between sub basins. The larger magnitude 10-year design event has a broadly similar response, though in specific cases (FRAAR and BRNFS) the magnitude of the design event is expected to increase monotonically throughout the coming century. In most cases, the magnitude of the 100-year event is expected to exceed the baseline value throughout the century, although the response over time is not always monotonic. In certain cases, the range in the 100-year change factor does dip below 1.0 early in the century (PRABD and PRAPR).

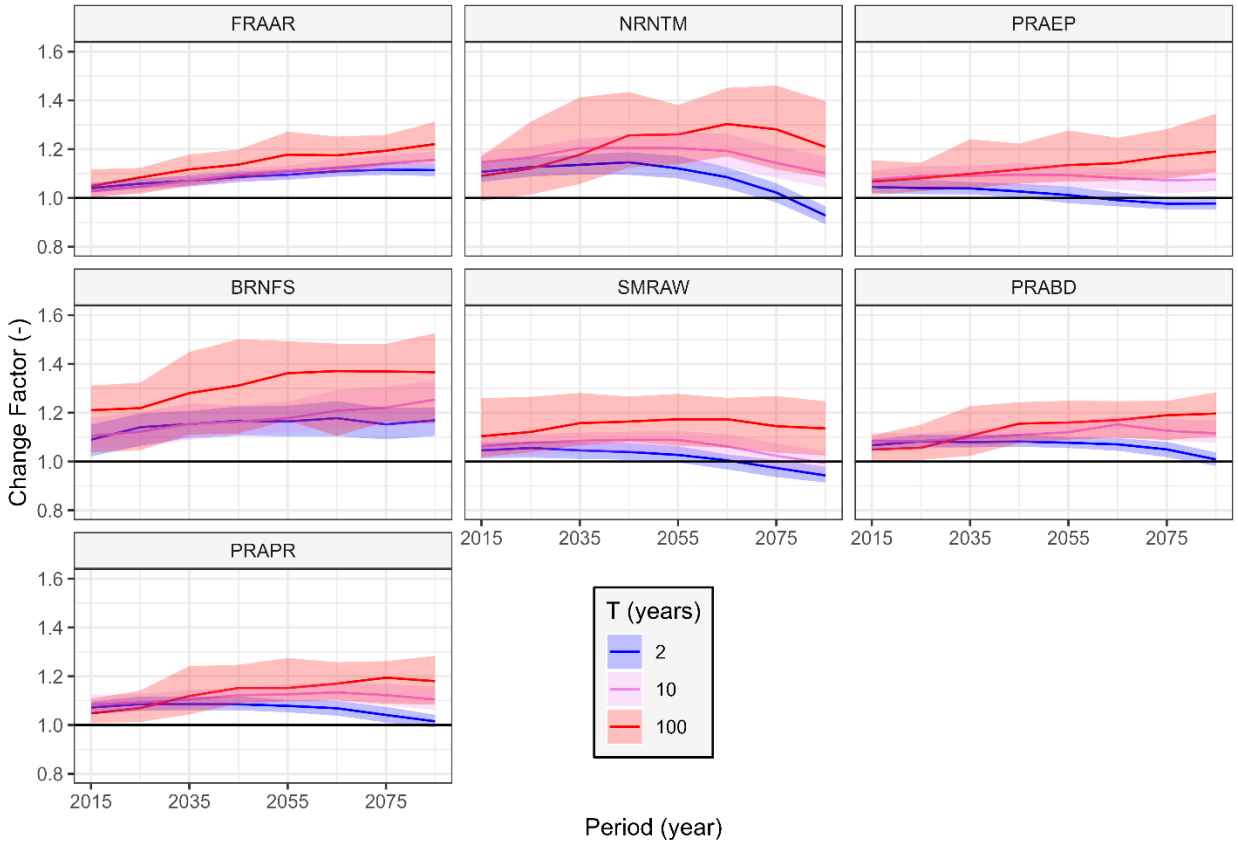

Figure 9. Change factors versus period, where the x-axis shows the mid-point of each period, for three quantiles at the outlets of six sub-basins and the Peace River basin. Change factors are estimated as the ratio of future value to historic value in the baseline period, where the baseline period is 1951-2000. Change factors of the median are given by the solid lines and the ribbons show the 95% confidence intervals.

5.3 Chilcotin Update

As discussed in Schnorbus and Sun (2022), initial VIC-GL streamflow simulation in the Chilcotin sub-basin was very poor. This was due to an overestimation of runoff arising from poor specification of the glacier state used to initialize the simulations. Specifically, simulations began with too much glacier volume such that the loss of glacier mass and glacier contribution to streamflow over time was exaggerated. This ultimately led to spurious and/or overly sensitive changes and trends in the annual maximum peak flow in the affected grid cells. This problem has been fixed by re-running the hydrologic projections using more a more realistic initialization of glacier area and thickness based on the regional glacier modelling of Clarke et al. (2015). The area affected by the update includes all grid cells upstream of the Chilko River at Redstone and the Taseko River at the outlet of Taseko Lake, as well as all downstream cells in the main stem of the Chilcotin River to its confluence with the Fraser. Updated results for projected peak flows and change factors are provided in Appendix B.

6 Discussion, Uncertainties and Limitations

6.1 Uncertainty in the Modelling Chain

Hydrologic projections are subject to uncertainties arising from the need to make choices regarding the various components of the modelling chain (Figure 4). And results are affected by the choice of emissions trajectory, GCM, downscaling approach, hydrology model structure, model calibration approach, methodology for estimating flood quantiles, and the various data sets used for model parametrization and calibration (Chegwidden et al., 2019; Curry et al., 2019; Queen et al., 2021; Schnorbus and Curry, 2019; Schoeneberg and Schnorbus, 2020). When using results from this study one should take careful consideration of the uncertainties and limitations inherent in the various modelling choices, which we discuss in the remainder of this section.

The actual trajectory of greenhouse gas emission that will occur during the 21st century is unknown. This uncertainty is addressed by using scenarios to capture a range of plausible emissions trajectories, which have been represented by the Representative Concentration Pathways (RCPs), of which there are four, RCP 2.6, 4.5, 6.0 and 8.5 (where the numbers refer to their peak radiative forcing at the end of the 21st century in W/m^2). The CanESM2 Large Ensemble is based solely on RCP 8.5, which has the highest radiative forcing of the four RCPs available.

Modelling the global climate response to radiative forcing includes two sources of uncertainty which can affect the possible range in future extremes. Differences between GCM structure (model numerics, resolution, process representation, parametrization, etc.) results in a range of climate responses to a given radiative forcing, resulting in so-called structural uncertainty. A second source of uncertainty is internal or natural climate variability, which refers to climate variations over time resulting from natural causes. We generally concern ourselves with unforced variations, which are internally generated redistributions of energy within the system that occur without changes in external factors, such as manifested by the El Niño/ Southern Oscillation. By only using ensemble results for the CanESM2 model, the spread of different runs can be attributed to internal variability only (Dai and Bloecker, 2019; Mahmoudi et al., 2021) and thus the generated hydrologic ensemble does not address GCM structural uncertainty.

The native-scale outputs of climate models and climate model output is of too coarse a resolution for most hydrologic applications and must be downscaled, often using statistical methods. Users must choose from a wide number of algorithms and target data sets, where the representation of precipitation and hydrologic extremes can be sensitive to the choice of downscaling method (Gutmann et al., 2014; Werner and

Cannon, 2016). Users should also be aware of the limitations that result from assumptions that need to be made in the statistical downscaling process. Like all statistical downscaling approaches, BCCAQv2 assumes that the quantile-mapping relationships that are established based on an observed target dataset and climate model simulated data for the historical training period continue to be valid in a climate change context. In addition, errors in the chosen target data set may introduce artefacts into the downscaling process.

The modelling chain used in this study is only designed to specifically address uncertainty due to climate variability, as it utilizes only a single emissions trajectory, GCM, downscaling scheme (trained to a single target data set), hydrology model (with one attempt at calibration) and routing model. However, recent research concludes that the choice of emissions scenario and GCM structural uncertainty tends to provide the largest source of uncertainty in hydrologic projections, and that the remaining sources of uncertainty are relatively small in comparison (Chegwidden et al., 2019; Hattermann et al., 2018; Her et al., 2019; Queen et al., 2021; Schoeneberg and Schnorbus, 2020; Sharma et al., 2018). In this context it is instructive to understand how well the range in CanESM2-based hydrologic projections compares to the range produced if a larger set of GCMs were used. In the pilot study Schoeneberg et al. (2021) explored this issue by comparing annual maximum peak flows generated from the CanESM2 large ensemble (45 realizations) with those simulated using the PCIC6 ensemble, which is composed of six GCMs, some with multiple runs, for total of 15 ensemble members. Even though the CanESM2 large ensemble is designed only to address internal climate variability, results show that the spread of the CanESM2 large ensemble is comparable to (and even larger than) the spread captured by the PCIC6 ensemble. Also, the direction of trend of the ensemble medians of annual maximum flow over the coming century is identical between ensembles in all sub basins, although and CanESM2 has larger positive and smaller (less negative) increasing and decreasing trends, respectively, than PCIC6. It should also be noted that the model spread in the raw CanESM2-LE is likely diminished as a result of postprocessing model output with BCCAQv2 (via the calibration of model output to a single collection of gridded observations).

With access to sufficiently large sample sizes, one can estimate quantile values directly from the empirical density function that are unbiased. This is the distinct advantage of using the CanESM2 large ensemble as the basis for this work, wherein quantiles for each analysis period are estimated using a sample of 1350 identically distributed peak flow events. A comparison of quantile estimation using both the GEV approach and the direct empirical approach was conducted during the pilot study (Schoeneberg et al., 2021) and confirmed that the parametric GEV approach produces biased estimates, particularly for large events. Nevertheless, the tradeoff for unbiased estimates is that the empirical quantiles have more variance and require a larger confidence interval than the corresponding GEV-based.

6.2 Interpreting Results and VIC-GL Limitations

VIC-GL's streamflow performance in the Peace overall is quite strong, and the representation of general streamflow signals (e.g., total volume, seasonality of low and high flow, low frequency variability) is accurate (Schnorbus, 2020). This lends confidence that the physical mechanisms that generate streamflow in the Peace are realistically simulated. However, simulation of annual maximum peak flow events represents a considerably harder challenge as accurate simulation over short times scales is very sensitive to model error and uncertainty in streamflow routing, forcing data (rainfall intensity or melt energy), snow dynamics, and storage dynamics (snow and soil). This is apparent when comparing model performance for general streamflow signals (NSE, KGE, Bias, Section A.1, Appendix A) to more specific peak flow metrics (Section A.2, Appendix A). Differences between observed and simulated peak flow magnitude can be very large, and VIC-GL is only able to match observed peak flow distributions at 5 of 26 evaluated sites (see Table A1 in the Appendix). The large uncertainties associated with observations of

peak flow events, for which errors can exceed ±30% (Di Baldassarre and Montanari, 2009; Horner et al., 2018), also affects model calibration and makes the interpretation of evaluation metrics and the objective assessment of model performance very difficult.

The physically based nature of the VIC-GL model lends some confidence that, over most of the combined Fraser and Peace study area the simulated peak flow changes reflect a physically realistic representation of the hydrologic response to climate change. However, due to the possible lack of representation of important hydrologic processes uniquely affecting runoff on the Interior Plains (see Appendix A for discussion), confidence is lower regarding the ability of VIC-GL to correctly represent the impact of climate change on peak flows in this region. One should also be aware that different choices regarding the model structure (level of abstraction, grid resolution, model physics, etc.), model parametrization, and calibration method (including data used to both force and constrain the model) can lead to a wide range in future projections (Chegwidden et al., 2019).

For calibration purposes the Peace and Fraser basins was divided into sub-basins based on the location of hydrometric sites. This sub-division represents a trade-off between number of calibration sites and available record lengths; longer record lengths (but with fewer sites) include more hydro-climate variability to train the model robustly whereas more sites (with shorter records) allow for a more realistic spatial variation in the model parameters. Calibration and parameter selection was conducted independently on each individual sub-basin. This approach, although computationally efficient, introduces artifacts into the spatial pattern in peak flow change. These calibration artifacts appear as abrupt changes in the sign of the response between grid cells that align with sub-basin boundaries used for model calibration (e.g., Figure 7). These artifacts tend to be more pronounced in the drier parts of the Peace and Fraser basins (where absolute changes may be small, but relative changes are large). This reinforces that relative peak flow changes are sensitive to model parameter choices and that parameter selection and calibration set-up introduce noise, notably at the model grid scale.

The resolution of the VIC-GL model also offers challenges in the interpretation of streamflow values and peak flow changes. Each grid cell can only have a single flow direction and a single channel, which imposes substantial simplification of the drainage system. This means that as drainage area decreases the modelled channel network (and resultant streamflow) becomes increasingly more abstract in terms of representing the detailed spatial structure of the drainage network. Also, with increasingly smaller drainage areas, the relative coarseness of the model resolution increases and the ability to accurately represent basin morphology and area (and, hence, runoff volume) degrades.

As mentioned in the previous section, a further limitation is that while the results are based on a large ensemble of climate change simulations, it is an ensemble from a single climate model using a single future forcing prescription. In addition, the climate model simulations have been downscaled using a single downscaling method trained against a particular gridded training dataset. Consequently, the full range of uncertainty in the derived design flows and change factors is certainly wider than that considered in this work. Nevertheless, despite the limitations, the information on projected design flow changes that is obtained should help to illuminate the potential impacts of climate change on design flow changes We reiterate that the physically based nature of the model does provide some level of confidence that it is responding in a plausible way to changes in the water balance and accompanying hydrological regime to projected climate changes. It would not perhaps be prudent for an engineer to alter design values from current values based directly on these results, but due diligence presumably imposes the requirement to think seriously about the implications of projected design value changes, even if uncertain.

7 Conclusions

PCIC has completed a project to quantify design flood values (2-, 20-, 50-, 100- and 200-year events) for historical and future periods and make them accessible as a gridded product via PCIC's Climate Explorer tool. This work represents a continuation of the work reported by Schoeneberg et al. (2021) and Schnorbus and Sun (2022) and uses a spatial domain that includes the original 234,000 km^2 Fraser River basin, but with the addition of gridded design values for the Peace River basin above Peace River, AB (194,000 km^2). Results are provided for every model grid cell in the domain at a spatial resolution of 0.0625°, and design flood values for each grid are based on streamflow routed from the area upstream of the selected cell. Hence, watershed areas range from ~30 km^2 (i.e., the area of a single headwater grid cell) to ~234,000 km^2. Flood design values have been provided at a temporal discretization based on 30-year sliding windows centered every 10-years on 2015 (2001-2030), 2025 (2011-2040), 2035 (2021-2050), 2045 (2031-2060), 2055 (2041-2070), 2065 (2051-2080), 2075 (2061-2090), 2085 (2071-2100). This work takes advantage of hydrologic projections produced by PCIC using the VIC-GL hydrology model driven with the CanESM2 50-member large ensemble (CanESM2-LE), which allows for statistically robust estimation of large return-period events. Change factors, ratios of future value to historic value, to represent projected changes in peak flow design values. Change factors can then be applied to scale design values derived directly from streamflow observations.

By using the CanESM2 large ensemble global climate simulations, but with only a single emissions trajectory, GCM, downscaling scheme (trained to a single target data set), hydrology model (with one attempt at calibration), and routing model, the modelling chain used in this study is only designed to specifically address uncertainty due to climate variability. Despite being limited to only a single hydrology model, the performance of VIC-GL is such that the simulated peak flow changes generally reflect a physically realistic representation of the hydrologic response to climate change over much of the combined Fraser and Peace study domain. However, the noted poor model performance in the Interior Plains physiographic region (i.e., Peace River east of the Rocky Mountains) requires caution when interpreting results from this portion of the domain. Results in general can be subject to high uncertainty, and results at the individual grid scale can be subject to considerable noise.

8 References

Alaya, M.A.B., Zwiers, F., Zhang, X., 2020. An Evaluation of Block-Maximum-Based Estimation of Very Long Return Period Precipitation Extremes with a Large Ensemble Climate Simulation. J. Clim. 33, 6957–6970. https://doi.org/10.1175/JCLI-D-19-0011.1

Arora, V.K., Cannon, A.J., 2018. A brief background on climate models: the source of future climate information. In: P. Mukhopadhyaya (ed.), 1st International Conference on New Horizons in Green Civil Engineering (NHICE-01), Victoria, BC, Canada, April 25-27, 2018. ISBN: 978-1-55058-620-6. p. 348-356.

Arora, V.K., Scinocca, J.F., Boer, G.J., Christian, J.R., Denman, K.L., Flato, G.M., Kharin, V.V., Lee, W.G., Merryfield, W.J., 2011. Carbon emission limits required to satisfy future representative concentration pathways of greenhouse gases. Geophys. Res. Lett. 38. https://doi.org/10.1029/2010GL046270

Baret, F., Weiss, M., Lacaze, R., Camacho, F., Makhmara, H., Pacholcyzk, P., Smets, B., 2013. GEOV1: LAI and FAPAR essential climate variables and FCOVER global time series capitalizing over existing products. Part1: Principles of development and production. Remote Sens. Environ. 137, 299–309. https://doi.org/10.1016/j.rse.2012.12.027

BCMoTI, 2019. Technical Circular T-04/19. Resilient Infrastructure Engineering Design - Adaptation to the Impacts of Climate Change and Weather Extremes.

BCMoTI, Nodelcorp Consulting Inc., Pacific Climate Impacts Consortium, 2014. Review and Analysis of Climate Change Vulnerability Assessments of Canadian Water Management and Drainage Infrastructure. Revision 2.

Camacho, F., Cernicharo, J., Lacaze, R., Baret, F., Weiss, M., 2013. GEOV1: LAI, FAPAR essential climate variables and FCOVER global time series capitalizing over existing products. Part 2: Validation and intercomparison with reference products. Remote Sens. Environ. 137, 310–329. https://doi.org/10.1016/j.rse.2013.02.030

Cannon, A.J., Jeong, D.I., Zhang, X., Zwiers, F.W., 2020. , in: Chapter 2 in CLIMATE-RESILIENT BUILDINGS & CORE PUBLIC INFRASTRUCTURE: An Assessment of the Impact of Climate Change on Climatic Design Data in Canada. Environment and Climate Change Canada. DRAFT. Victoria, BC, Canada, p. 15 pp.

Cannon, A.J., Sobie, S.R., Murdock, T.Q., 2015. Bias Correction of GCM Precipitation by Quantile Mapping: How Well Do Methods Preserve Changes in Quantiles and Extremes? J. Clim. 28, 6938–6959. https://doi.org/10.1175/JCLI-D-14-00754.1

Chegwidden, O.S., Nijssen, B., Rupp, D.E., Arnold, J.R., Clark, M.P., Hamman, J.J., Kao, S.-C., Mao, Y., Mizukami, N., Mote, P.W., Pan, M., Pytlak, E., Xiao, M., 2019. How Do Modeling Decisions Affect the Spread Among Hydrologic Climate Change Projections? Exploring a Large Ensemble of Simulations Across a Diversity of Hydroclimates. Earths Future 7, 623–637. https://doi.org/10.1029/2018EF001047

Cherkauer, K.A., Bowling, L.C., Lettenmaier, D.P., 2003. Variable infiltration capacity cold land process model updates. Glob. Planet. Change 38, 151–159.

Clarke, G.K.C., Jarosch, A.H., Anslow, F.S., Radić, V., Menounos, B., 2015. Projected deglaciation of western Canada in the twenty-first century. Nat. Geosci. 8, 372–377. https://doi.org/10.1038/ngeo2407

Curry, C.L., Islam, S.U., Zwiers, F.W., Déry, S.J., 2019. Atmospheric Rivers Increase Future Flood Risk in Western Canada's Largest Pacific River. Geophys. Res. Lett. 46, 1651–1661. https://doi.org/10.1029/2018GL080720

Dai, A., Bloecker, C.E., 2019. Impacts of internal variability on temperature and precipitation trends in large ensemble simulations by two climate models. Clim. Dyn. 52, 289–306. https://doi.org/10.1007/s00382-018-4132-4

Danielson, J.J., Gesch, D.B., 2011. Global Multi-resolution Terrain Elevation Data 2010 (GMTED2010). U.S. Geological Survey Open-File Report 2011–1073. U.S. Department of the Interior, U.S. Geological Survey, National Geospatial-Intelligence Agency.

Di Baldassarre, G., Montanari, A., 2009. Uncertainty in river discharge observations: a quantitative analysis. Hydrol. Earth Syst. Sci. 13, 913–921. https://doi.org/10.5194/hess-13-913-2009

Fyfe, J.C., Derksen, C., Mudryk, L., Flato, G.M., Santer, B.D., Swart, N.C., Molotch, N.P., Zhang, X., Wan, H., Arora, V.K., Scinocca, J., Jiao, Y., 2017. Large near-term projected snowpack loss over the western United States. Nat. Commun. 8, 14996. https://doi.org/10.1038/ncomms14996

Gao, C., Booij, M.J., Xu, Y.-P., 2020. Assessment of extreme flows and uncertainty under climate change: disentangling the contribution of RCPs, GCMs and internal climate variability. Hydrol. Earth Syst. Sci. Discuss. 1–28. https://doi.org/10.5194/hess-2020-25

Global Soil Data Task, 2014. Global Soil Data Products CD-ROM Contents (IGBP-DIS). ORNL DAAC, doi:https://doi.org/10.3334/ORNLDAAC/565.

Government of Canada, 2019. The Canadian Earth System Model Large Ensembles [WWW Document]. Opendat Can. URL https://open.canada.ca/data/en/dataset/aa7b6823-fd1e-49ff-a6fb-68076a4a477c (accessed 7.19.19).

Gudmundsson, G.H., Krug, J., Durand, G., L., Favier., Gagliardini, O., 2012. The stability of grounding lines on retrograde slopes. Cryosphere Discuss. 6, 2597–2619.

Gutmann, E., Pruitt, T., Clark, M.P., Brekke, L., Arnold, J.R., Raff, D.A., Rasmussen, R.M., 2014. An intercomparison of statistical downscaling methods used for water resource assessments in the United States. Water Resour. Res. 50, 7167–7186. https://doi.org/10.1002/2014WR015559

Hattermann, F.F., Vetter, T., Breuer, L., Su, B., Daggupati, P., Donnelly, C., Fekete, B., Flörke, F., Gosling, S.N., Hoffmann, P., Liersch, S., Masaki, Y., Motovilov, Y., Müller, C., Samaniego, L., Stacke, T., Wada, Y., Yang, T., Krysnaova, V., 2018. Sources of uncertainty in hydrological climate impact assessment: a cross-scale study. Environ. Res. Lett. 13, 015006. https://doi.org/10.1088/1748-9326/aa9938

Her, Y., Yoo, S.-H., Cho, J., Hwang, S., Jeong, J., Seong, C., 2019. Uncertainty in hydrological analysis of climate change: multi-parameter vs. multi-GCM ensemble predictions. Sci. Rep. 9, 4974. https://doi.org/10.1038/s41598-019-41334-7

Hiebert, J., Cannon, A., Murdock, T., Sobie, S., Werner, A., 2018. ClimDown: Climate Downscaling in R, Journal of Open Source Software. https://doi.org/10.21105/joss.00360

Horner, I., Renard, B., Le Coz, J., Branger, F., McMillan, H.K., Pierrefeu, G., 2018. Impact of Stage Measurement Errors on Streamflow Uncertainty. Water Resour. Res. 54, 1952–1976. https://doi.org/10.1002/2017WR022039

Hunter, R.D., Meentemeyer, R.K., 2005. Climatologically Aided Mapping of Daily Precipitation and Temperature. J. Appl. Meteorol. 44, 1501–1510. https://doi.org/10.1175/JAM2295.1

Kirchmeier-Young, M.C., Zhang, X., 2020. Human influence has intensified extreme precipitation in North America. Proc. Natl. Acad. Sci. https://doi.org/10.1073/pnas.1921628117

Kirchmeier-Young, M.C., Zwiers, F.W., Gillett, N.P., 2017a. Attribution of Extreme Events in Arctic Sea Ice Extent. J. Clim. 30, 553–571. https://doi.org/10.1175/JCLI-D-16-0412.1

Kirchmeier-Young, M.C., Zwiers, F.W., Gillett, N.P., Cannon, A.J., 2017b. Attributing extreme fire risk in Western Canada to human emissions. Clim. Change 1–15. https://doi.org/10.1007/s10584-017-2030-0

Kushner, P.J., Mudryk, L.R., Merryfield, W., Ambadan, J.T., Berg, A., Bichet, A., Brown, R., Derksen, C., Déry, S.J., Dirkson, A., Flato, G., Fletcher, C.G., Fyfe, J.C., Gillett, N., Haas, C., Howell, S., Laliberté, F., McCusker, K., Sigmond, M., Sospedra-Alfonso, R., Tandon, N.F., Thackeray, C., Tremblay, B., Zwiers, F.W., 2018. Canadian snow and sea ice: assessment of snow, sea ice, and related climate processes in Canada's Earth system model and climate-prediction system. The Cryosphere 12, 1137–1156. https://doi.org/10.5194/tc-12-1137-2018

Li, C., Zwiers, F., Zhang, X., Chen, G., Lu, J., Li, G., Norris, J., Tan, Y., Sun, Y., Liu, M., 2019. Larger Increases in More Extreme Local Precipitation Events as Climate Warms. Geophys. Res. Lett. 46, 6885–6891. https://doi.org/10.1029/2019GL082908

Li, C., Zwiers, F., Zhang, X., Li, G., Sun, Y., Wehner, M., 2020. Changes in annual extremes of daily temperature and precipitation in CMIP6 models. J. Clim. 1, 1–61. https://doi.org/10.1175/JCLI-D-19-1013.1

Liang, X., Lettenmaier, D.P., Wood, E.F., Burges, S.J., 1994. A simple hydrologically based model of land-surface water and energy fluxes for general-circulation models. J. Geophys. Res.-Atmospheres 99, 14415–14428. https://doi.org/10.1029/94JD00483

Liang, X., Wood, E.F., Lettenmaier, D.P., 1996. Surface soil moisture parameterization of the VIC-2L model: Evaluation and modification. Glob. Planet. Change, Soil Moisture Simulation 13, 195–206. https://doi.org/10.1016/0921-8181(95)00046-1

Lohmann, D., Raschke, E., Nijssen, B., Lettenmaier, D.P., 1998. Regional scale hydrology: I. Formulation of the VIC-2L model coupled to a routing model. Hydrol. Sci. J. 43, 131–141. https://doi.org/10.1080/02626669809492107

Mahmoudi, M.H., Najafi, M.R., Singh, H., Schnorbus, M., 2021. Spatial and temporal changes in climate extremes over northwestern North America: the influence of internal climate variability and external forcing. Clim. Change 165, 14. https://doi.org/10.1007/s10584-021-03037-9

Maurer, E.P., Hidalgo, H.G., Das, T., Dettinger, M.D., Cayan, D.R., 2010. The utility of daily large-scale climate data in the assessment of climate change impacts on daily streamflow in California. Hydrol Earth Syst Sci 14, 1125–1138. https://doi.org/10.5194/hess-14-1125-2010

Natural Resources Canada/ The Canada Centre for Mapping and Earth Observation (NRCan/CCMEO), United States Geological Survey (USGS), Insituto Nacional de Estadística y Geografía (INEGI), Comisión Nacional para el Conocimiento y Uso de la Biodiversidad (CONABIO), and Comisión Nacional Forestal (CONAFOR), 2013. 2013: 2010 North American Land Cover at 250 m spatial resolution.

Pfeffer, W.T., Arendt, A.A., Bliss, A., Bolch, T., Cogley, J.G., Gardner, A.S., Hagen, J.-O., Hock, R., Kaser, G., Kienholz, C., Miles, E.S., Moholdt, G., Mölg, N., Paul, F., Radić, V., Rastner, P., Raup, B.H., Rich, J., Sharp, M.J., Consortium, T.R., 2014. The Randolph Glacier Inventory: a globally complete inventory of glaciers. J. Glaciol. 60, 537–552. https://doi.org/10.3189/2014JoG13J176

Queen, L.E., Mote, P.W., Rupp, D.E., Chegwidden, O., Nijssen, B., 2021. Ubiquitous increases in flood magnitude in the Columbia River basin under climate change. Hydrol. Earth Syst. Sci. 25, 257–272. https://doi.org/10.5194/hess-25-257-2021

R Core Team, 2019. R: A Language and Environment for Statistical Computing. R Foundation for Statistical Computing, Vienna, Austria.

Schnorbus, M., 2018. VIC Glacier: Description of VIC model changes and updates (PCIC Internal Report). Pacific Climate Impacts Consortium, Victoria, BC.

Schnorbus, M., 2017. VICGL Model Calibration (PCIC Internal Report). Pacific Climate Impacts Consortium, Victoria, BC.

Schnorbus, M.A., 2021. Model Validation Report for the Fraser River Watershed. Pacific Climate Impacts Consortium, University of Victoria, Victoria, BC.

Schnorbus, M.A., 2020. VIC Glacier (VIC-GL): Model Set-up and Deployment for the Peace, Fraser, and Columbia (VIC-GL Deployment No. Volume 6), VIC Generation 2 Deployment Report. Pacific Climate Impacts Consortium, University of Victoria, Victoria, B.C.

Schnorbus, M.A., Curry, C.L., 2019. Climate Change Scenario Modelling for the Fraser River Watershed Phase 2 - Final Report. Pacific Climate Impacts Consortium, University of Victoria.

Schnorbus, M.A., Sun, Q., 2022. Future Design Flood Values in the Fraser River Basin Using the CanESM2-LE: Final Report to "Revision and Expansion of Extreme Streamflow Design Value Projection Online Tool ". Pacific Climate Impacts Consortium, University of Victoria, Victoria, B.C.

Schoeneberg, A.T., Schnorbus, M.A., 2020. Exploring the Strength and Limitations of PCIC's CMIP5 Hydrologic Scenarios. Pacific Climate Impacts Consortium, University of Victoria, Victoria, BC, Canada.

Schoeneberg, A.T., Sun, Q., Schnorbus, M.A., 2021. Future Design Flood Values in the Upper Fraser River Basin using the CanESM2-LE: Final Report to "Pilot Study for Development of Streamflow Design Value Projections and Prototype Online Tool." Pacific Climate Impacts Consortium, University of Victoria, Victoria, BC.

Sharma, T., Vittal, H., Chhabra, S., Salvi, K., Ghosh, S., Karmakar, S., 2018. Understanding the cascade of GCM and downscaling uncertainties in hydro-climatic projections over India. Int. J. Climatol. 38, e178–e190. https://doi.org/10.1002/joc.5361

Simard, M., Pinto, N., Fisher, J.B., Baccini, A., 2011. Mapping forest canopy height globally with spaceborne lidar. J. Geophys. Res. Biogeosciences 116. https://doi.org/10.1029/2011JG001708

Sobie, S.R., Murdock, T.Q., 2017. High-Resolution Statistical Downscaling in Southwestern British Columbia. J. Appl. Meteorol. Climatol. 56, 1625–1641. https://doi.org/10.1175/JAMC-D-16-0287.1

Taylor, K.E., Stouffer, R.J., Meehl, G.A., 2011. An Overview of CMIP5 and the Experiment Design. Bull. Am. Meteorol. Soc. 93, 485–498. https://doi.org/10.1175/BAMS-D-11-00094.1

Todini, E., 1996. The ARNO rainfall—runoff model. J. Hydrol. 175, 339–382. https://doi.org/10.1016/S0022-1694(96)80016-3

Werner, A.T., Cannon, A.J., 2016. Hydrologic extremes – an intercomparison of multiple gridded statistical downscaling methods. Hydrol. Earth Syst. Sci. 20, 1483–1508. https://doi.org/10.5194/hess-20-1483-2016

Werner, A.T., Schnorbus, M.A., Shrestha, R.R., Cannon, A.J., Zwiers, F.W., Dayon, G., Anslow, F., 2019. A long-term, temporally consistent, gridded daily meteorological dataset for northwestern North America. Sci. Data 6, 180299. https://doi.org/10.1038/sdata.2018.299

Appendix A - Model Evaluation

A.1 Streamflow Evaluation

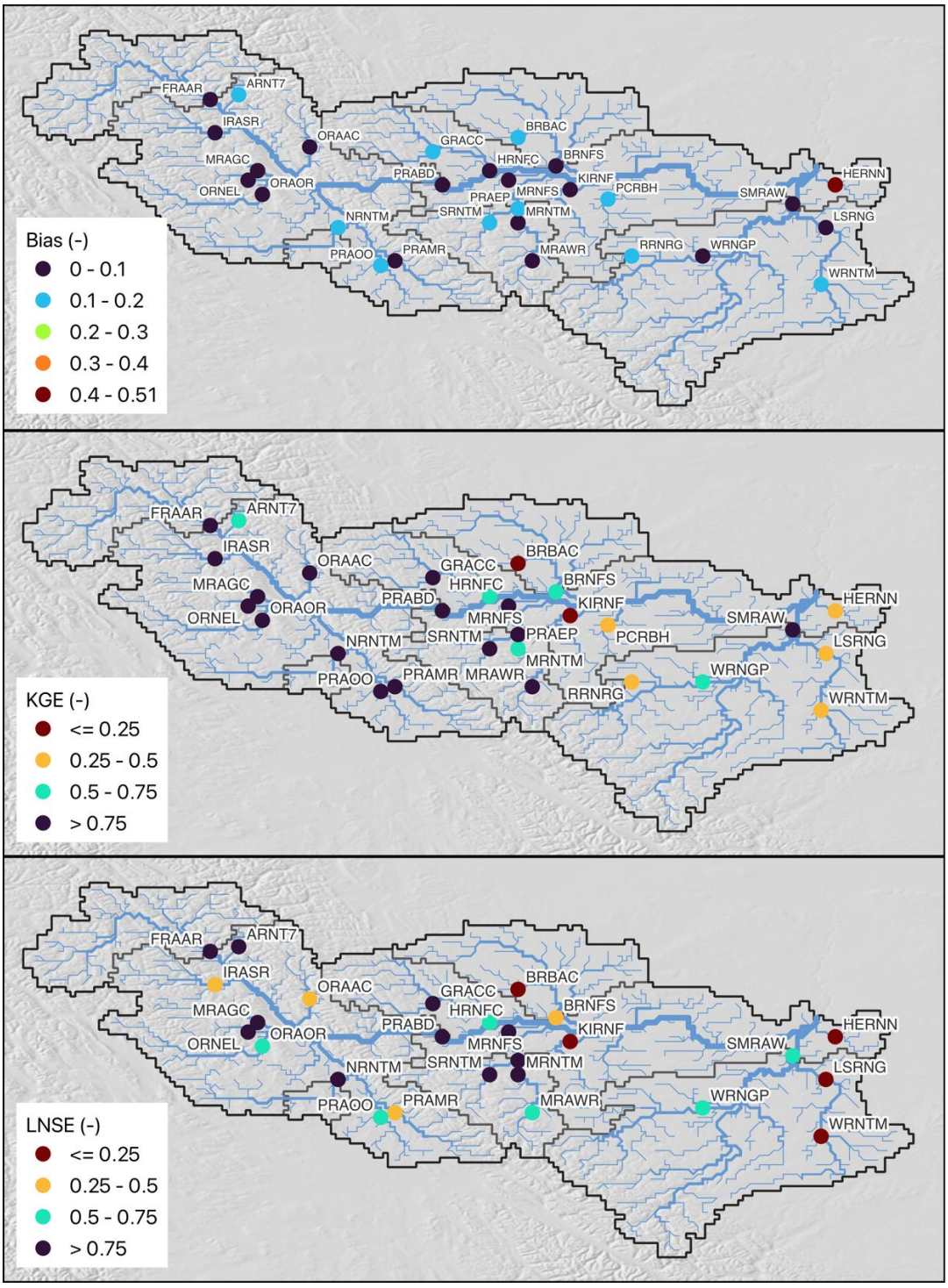

Figure A1. Metrics of streamflow *Bias* (top), *KGE* (middle) and *LNSE* (bottom) for the Peace Basin.

The general performance of the VIC-GL model in simulating streamflow is presented in Figure A1, which summarizes results for the Kling-Gupta Efficiency (*KGE*), Nash-Sutcliffe of log-transformed discharge (*LNSE*), and relative bias metrics for 28 locations corresponding to 27 Water Survey of Canada (WSC) locations and one (PRABD) BC Hydro project site. The reader is referred to Schnorbus (2020) for a description of the calibration and evaluation process and greater details on general model performance.

Streamflow bias is quite low, below 20% for most sites, and below 10% for more than half the sites in Figure A1. Model performance based on the KGE is also good with values at over half the sites exceeding 0.75 and most sites exceeding 0.50. Performance based on LNSE is not quite as strong, with less than half the sites having values exceeding 0.75, although values for most sites still exceed 0.50. Of note is that the poorer performing sites, particularly for KGE, tend to be located east of the Rocky Mountains.

A.2 Peak Flow Evaluation

In this section the performance of the VIC-GL model in simulating annual maximum peak flow events is evaluated. The evaluation is carried out by comparing annual maximum daily peak discharge events from both observation and model simulation, where model simulations were produced by forcing VIC-GL using the PNWNAmet observed meteorological data. Evaluations are limited to those Water Survey of Canada (WSC) stations where at least 30 observations of annual maximum peak flow were available between 1945 and 2012 (**Error! Reference source not found.**). The following metrics were used to evaluate peak flow model performance.

Relative Root Mean Square Error: this is the root mean square error (RMSE) normalized by the mean of the observations as

$$RRMSE = \frac{\sqrt{\frac{1}{N}\sum_{i=1}^{N}(S_i - O_i)^2}}{\bar{\bar{O}}}$$

where *S* and *O* are simulated and observed values, respectively and *N* is the sample size. This value is given as a fraction with a range of (0, ∞), where 0 denotes perfect performance (i.e., no error).

Normalized Root Mean Square Error: this is the root mean square error normalized by the standard deviation if the observations as

$$NRMSE = \frac{\sqrt{\frac{1}{N}\sum_{i=1}^{N}(S_i - O_i)^2}}{sd(O)}.$$

As per the *RRMSE*, the *NRMSE* is given as a fraction with a range (0, ∞), where 0 denotes perfect performance.

Model performance for annual maximum peak flow is summarized in Table A1. Results for root mean square error normalized to the observed mean (*RRMSE*) range from a best of 0.24 (MRAGC) to a worst of 16.28 (SRNTM). When normalized by the observed standard deviation (*NRMSE*), result range from a best of 1.13 (MRAGC) to a worst of 45.25 (SMRAW). Results for *KS_D* range from a best of 0.11

(MRAGC) to a worst of 1.00 (FRAAR, PERNT, PRAEP, SMRAW and SRNTM). When viewed spatially it is clear that model performance (**Error! Reference source not found.**), tends to exhibit a spatial gradient where the best model performance (lower *RRMSE* and *NRMSE*) occurs in the western, mountainous portion of the basin, whereas model performance tends to degrade when moving east onto the Interior Plains (Figure A2).

Scatterplots comparing observed versus simulated annual maximum peak flow data for selected sites is given in Figure A3. Four sites are chosen to help visualize the degree of agreement (or disagreement) for the range of RRMSE values found in Table A1. From the figure it is apparent that large RRMSE values are generally due to large biases between observed and simulated values.

In Figure A4 we compare the empirical cumulative distribution function of observed and simulated annual maximum peak flows for all the evaluation sites listed in Table 3. It is noted that model performance in replicating the observed cumulative distribution function is qualitatively quite good at several sites (i.e., KWRNW, MRAGC, NRNFS, ORNEL and PRAOO). However, it is also clear that the simulated annual maximum peak flows at many locations are either grossly overestimated (e.g., BRBAC, SRNTM and WRNTM) or grossly underestimated (e.g., BRNFS, FRAAR and PERNT). Again, with a few exceptions, the worst performing sites tend to be located on the Interior Plains east of the Continental Divide.

At present we have no explanation for this apparent degradation in model performance in the Interior Plains region, although we can speculate on two physical phenomena that are not explicitly represented in the hydrologic modelling process. Firstly, the rolling and undulating terrain of the Interior Plains results in a prevalence of small lakes and wetlands that are only intermittently integrated in the channel drainage network. This results in a dynamic surface drainage response that can have a highly non-linear effect on peak flow magnitude. Another possibility is omission of the effects of river ice and ice breakup on the magnitude of peak water level and discharge.

We also note that the apparent poor performance may be related to errors in the underlying PNWNAmet forcing data set used to both calibrate VIC-GL and train the BCCAQv2 statistical downscaling. The spatial density of long-term meteorological stations available in the interpolation of temperature and precipitation is quite low in the norther half of the province. So, although it would appear that PNWNAmet has accurate climatology, as suggested by the low streamflow bias (Figure A1), the spatial and temporal variability of meteorological events responsible for extreme streamflow may not be well represented.

Table A1. Peak flow evaluation statistics at Water Survey of Canada sites for the Peace River basin, where *N* is sample size, *RRMSE* is relative root mean square error (normalized by the observed mean), and *NRMSE* is the RMSE normalized by the observed standard deviation.

Basin	*N*	*RRMSE*	*NRMSE*
ARNT7	30	0.44	1.50
BRBAC	47	1.37	2.96
BRNFS	51	0.79	9.37
FRAAR	34	0.85	19.22
IRASR	35	0.43	2.85
KIRNF	52	1.23	2.75
KWRNW	34	0.26	1.15
LSRNG	50	0.85	7.70
MRAGC	37	0.24	1.13
MRAWR	35	0.42	2.59
MRNFS	33	2.92	3.41
MRNTM	35	0.62	5.91
NRNFS	37	0.46	1.19
NRNTM	32	0.52	4.26
ORAAC	32	0.42	2.17
ORAOR	37	0.58	5.73
ORNEL	32	0.25	1.01
PCRBH	39	1.75	4.00
PERNT	66	1.07	42.55
PRAEP	52	0.94	23.74
PRAMR	44	0.69	8.76
PRAOO	32	0.34	1.39
SMRAW	58	1.10	45.25
SRNTM	35	16.28	4.32
WRNGP	52	1.11	17.74
WRNTM	45	2.79	3.38

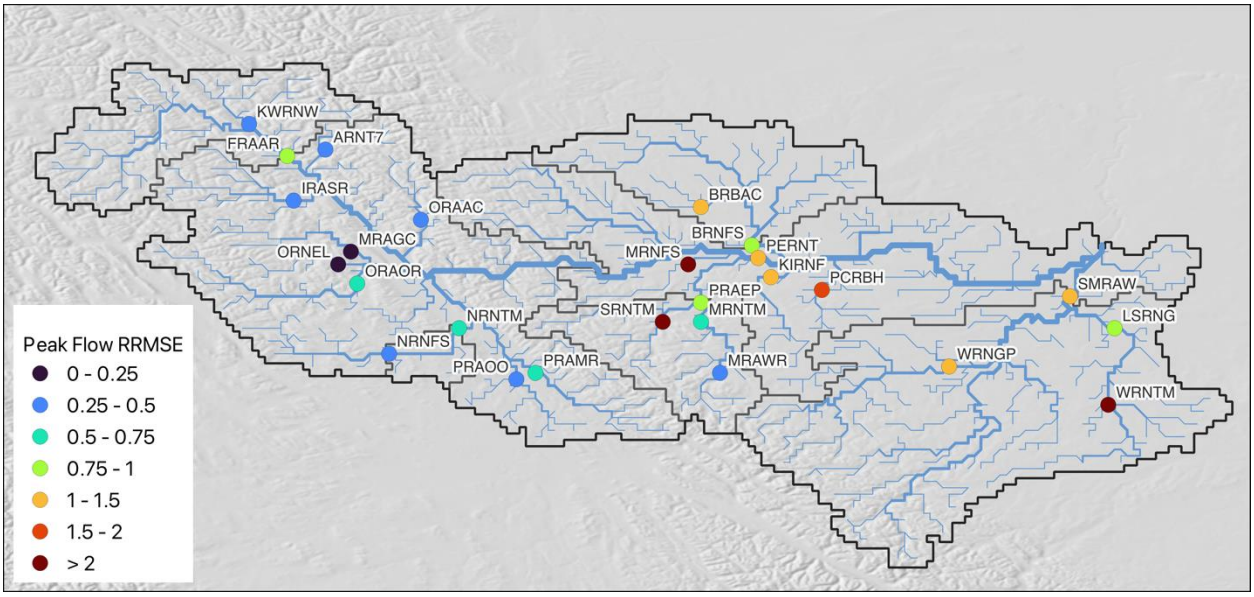

Figure A2. Peak Relative Root Mean Square Error results for the Peace Basin.

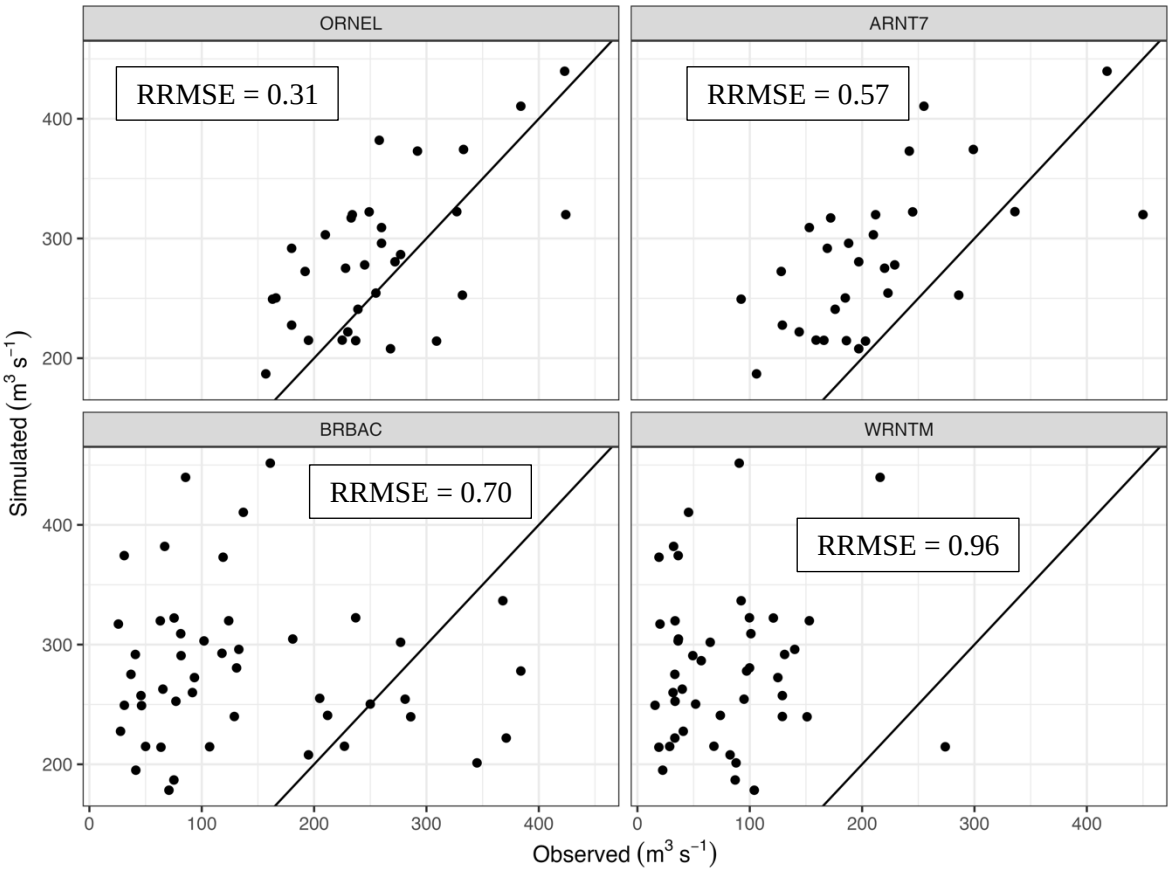

Figure A3. Scatterplot of observed versus simulated annual maximum peak discharge for four select calibration sites. Each panel shows the 1:1 and is labelled with the relative root mean square error (RRMSE).

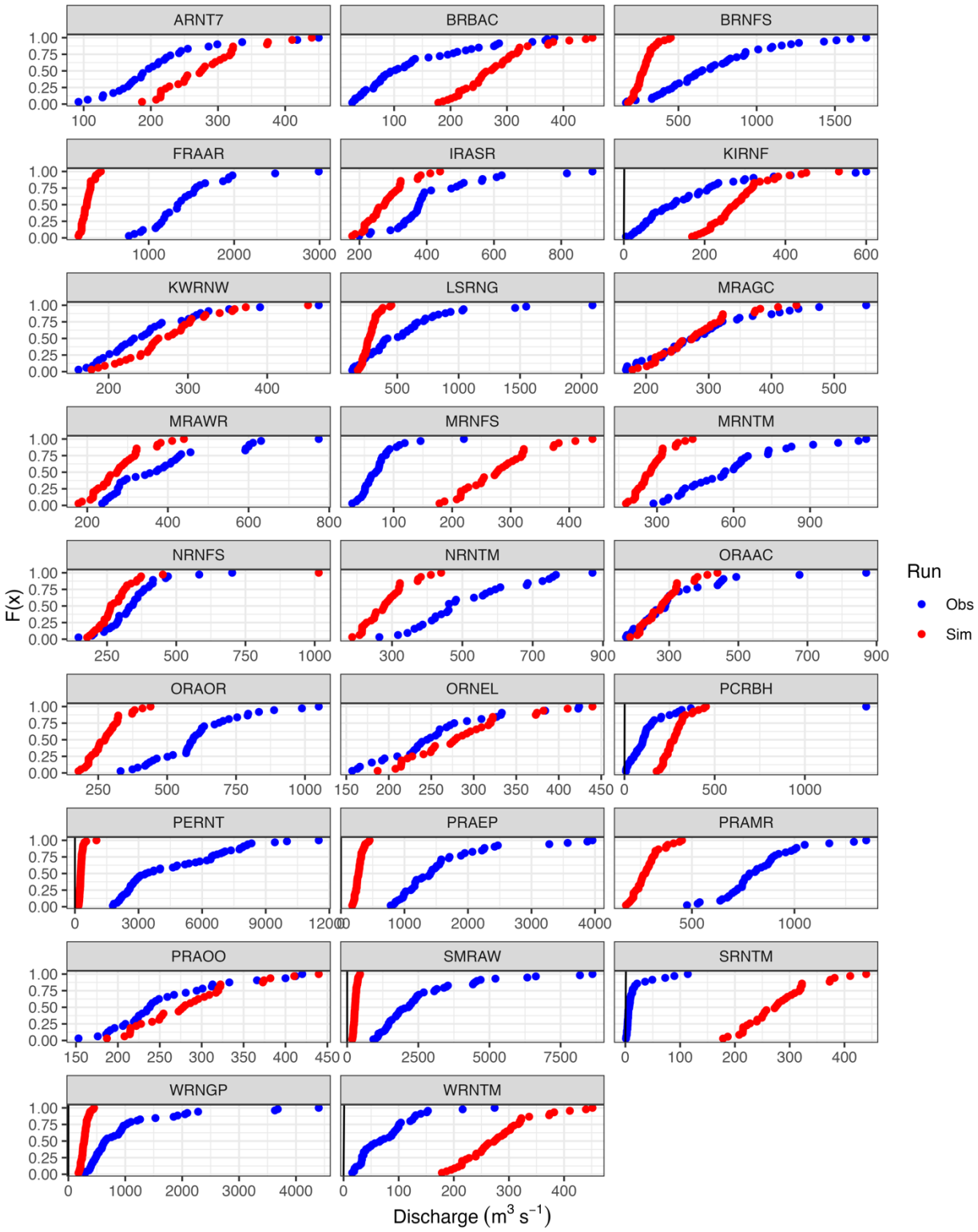

Figure A4. Empirical cumulative density function of observed and simulated annual maximum peak discharge for all sites in Table A1.

Appendix B – Chilcotin Update

In this section we reproduce two figures from Schnorbus and Sun (2022), but based on updated streamflow projections for the Chilcotin basin. Figure 10 shows flood frequency curves at several locations in the Fraser, the Stuart River near Fort St. James (STUAR), Nechako River at Isle Pierre (NECHI), Fraser River at Shelley (FRSSH), Chilcotin River above Big Creek (CHILB), Quesnel River at Quesnel (QUESQ), Fraser River above Texas Creek (FRSTX), Thompson River near Spences Bridge (THOMS) and Fraser River at the Mouth (FRSMT). Although the updated results for CHILB still show a negative projected trend in design flow magnitude, the magnitude of change is considerably smaller compared to the original results.

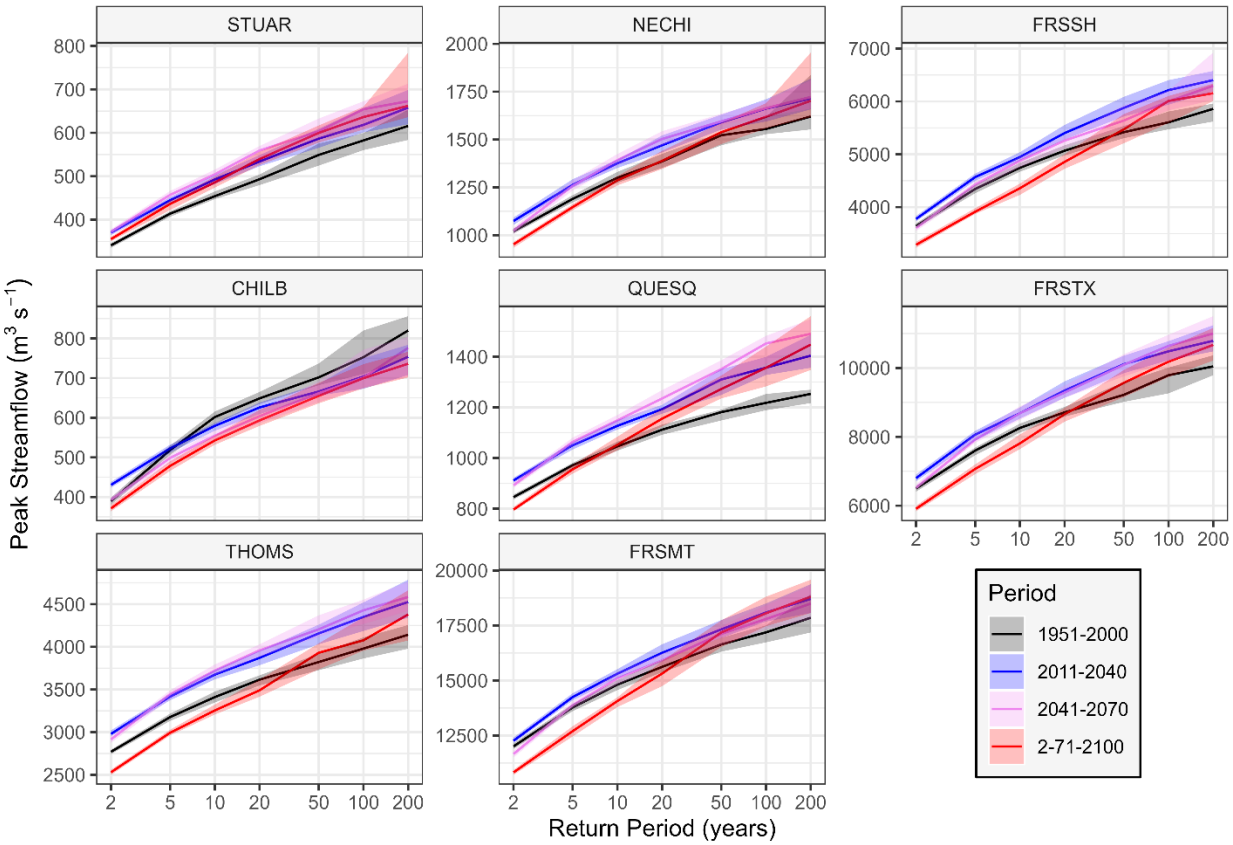

Figure 10. Reproduction if Figure 9 from Schnorbus and Sun (2022) showing flood frequency curves for several locations in the Fraser basin. Results are based on updated streamflow projections for the Chilcotin River below Big Creek (CHILB). The remaining sites are the Stuart River near Fort St. James (STUAR), Nechako River at Isle Pierre (NECHI), Fraser River at Shelley (FRSSH), Quesnel River at Quesnel (QUESQ), Fraser River above Texas Creek (FRSTX), Thompson River near Spences Bridge (THOMS) and Fraser River at the Mouth (FRSMT).

Figure 11 shows projected changes factors by period for the 2-, 10- and 100-year design events for the same locations. In contrast to the original results, changes factors for the 2-year event in the CHILB are positive throughout the coming century, although the magnitude of increase will have a declining trend. With the updated projections, the change factors for the 10-year and 100-year design events in CHILB will be largely unaffected. This still contrasts with the other seven locations, where change factors for the

10- and 100-year design events are expected to exceed 1 throughout the first 75 years of the century. Despite the adjustment made to the glacier initialization, projections still suggest that changes to design flow values in the CHILB will still be predominantly influenced by declining glacier melt.

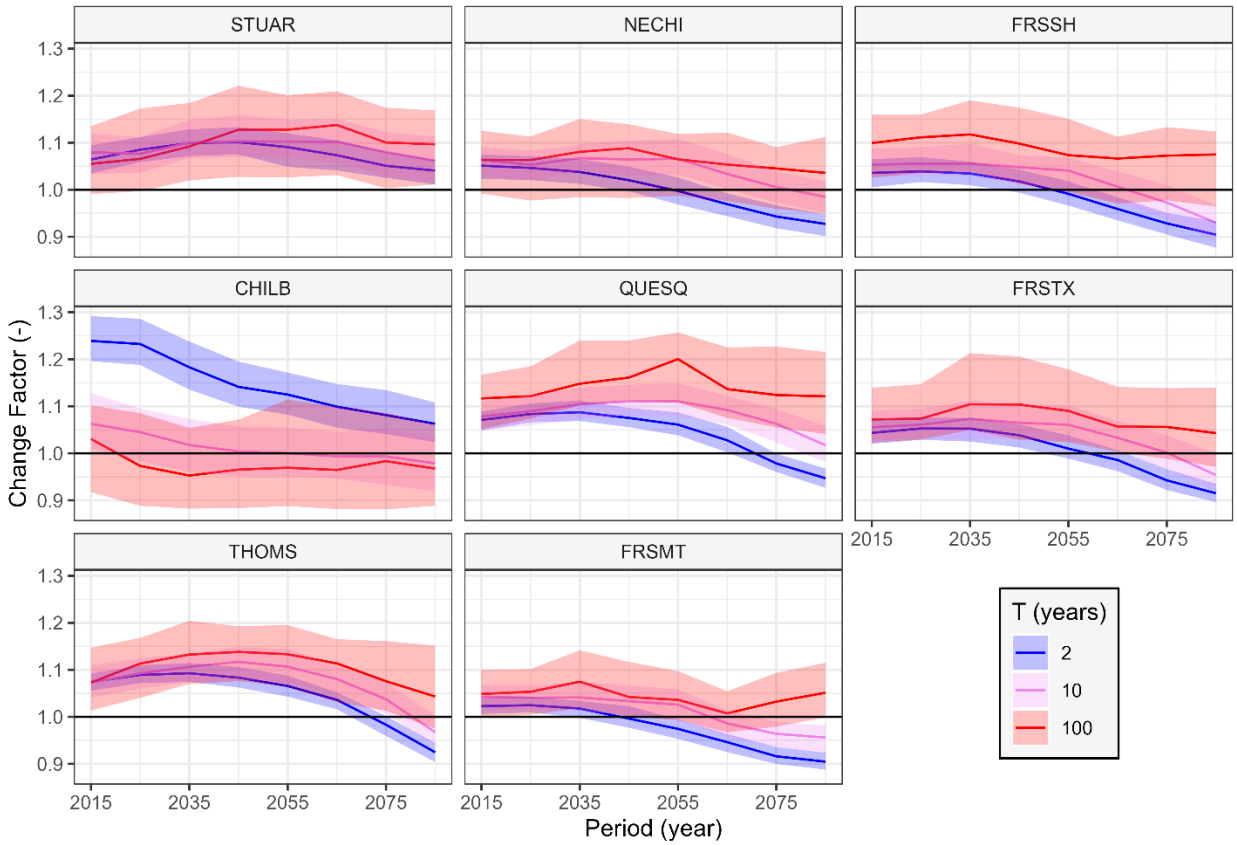

Figure 11. Reproduction of Figure 11 from Schnorbus and Sun (2022) change factors for different periods for several locations in the Fraser basin. Results are based on updated streamflow projections for the Chilcotin River below Big Creek (CHILB). The remaining sites are the Stuart River near Fort St. James (STUAR), Nechako River at Isle Pierre (NECHI), Fraser River at Shelley (FRSSH), Quesnel River at Quesnel (QUESQ), Fraser River above Texas Creek (FRSTX), Thompson River near Spences Bridge (THOMS) and Fraser River at the Mouth (FRSMT).